Received: 25 May 2018 | Revised: 19 September 2018 | Accepted: 21 September 2018

DOI: 10.1002/num.22324

RESEARCH ARTICLE

WILEY

Discontinuous Galerkin method for solving the black-oil problem in porous media

Loïc Cappanera | **Béatrice Rivière**

Department of Computational and Applied Mathematics, Rice University, Houston, Texas

Correspondence
Loïc Cappanera, Department of Computational and Applied Mathematics (CAAM), Rice University, 6100 Main St.-MS 134, Houston, TX 77005-1827.
Email: loic.cappanera@rice.edu

We introduce a new algorithm for solving the three-component three-phase flow problem in two-dimensional and three-dimensional heterogeneous media. The oil and gas components can be found in the liquid and vapor phases, whereas the aqueous phase is only composed of water component. The numerical scheme employs a sequential implicit formulation discretized with discontinuous finite elements. Capillarity and gravity effects are included. The method is shown to be accurate and robust for several test problems. It has been carefully designed so that calculation of appearance and disappearance of phases does not require additional steps.

KEYWORDS

black oil problem, capillary pressures, discontinuous Galerkin, gravity, heterogeneous porous media, phase appearance and disappearance

1 | INTRODUCTION

The three-phase three-component problem, also referred to as the black-oil problem in petroleum engineering, is a nonlinear system of coupled partial differential equations and algebraic equations. The formulation of the problem consists of the mass balance equations for each of the components and of closure relationships between the physical unknowns such as phase pressure, saturations and mass fractions. The resulting compositional model is in general used for a large number of components. In the black oil model, there are three components (water, oil, gas) and three phases (aqueous, liquid, vapor). We assume that the aqueous phase is comprised of the water component only and that mass transfer occurs between the liquid and vapor phase: the gas component can be dissolved in the liquid phase and the oil component can evaporate. One of the numerical challenges of multicomponent

multiphase flows is to efficiently treat the phase appearance and disappearance as components move from one phase to another one. The literature on black-oil model is vast and dates back from several decades. We refer the reader to classical books [1–3] and to the papers [4–11] for several approaches to solve the resulting nonlinear coupled system of equations. Once a set of primary unknowns is selected (among quantities such as phase pressure, global pressure, phase saturation, mass fraction, molar densities), the main approaches are the fully implicit approach that requires a Newton-based scheme [6], the IMPES approach in which the pressure is solved implicitely and saturation explicitely [4, 8] and the sequential approach that solves each equation implicitely and separately from the other ones [5, 9, 10]. The large number of proposed numerical algorithms in the literature is due to many technical differences in the details of each approach. It is also worth noting that not all papers address the full complexity of the multiphase flows and the effects of capillary pressure and gravity are sometimes neglected. Overall, when comparing cost versus accuracy and stability, it is well-accepted that the sequential approach is the most efficient method for large scale computations.

This paper's main contribution is to formulate a discontinuous Galerkin (DG) method for solving the three-phase three-component problem in two-dimensional and three-dimensional porous media. We start with the compositional model and introduce a new variable, the total mass fraction of gas, following [12]. The primary unknowns are the liquid pressure, the aqueous saturation and the total mass fraction of gas. We show that the proposed sequential implicit algorithm converges optimally for smooth solutions and that it is robust when phases disappear or appear. The main features of the numerical method are: (a) the use of weighted averages (see [13]); (b) the use of a subiterative scheme for higher accurary; (c) the use of upwind fluxes; and (d) the projection of the total velocity into H(div) conforming spaces (see [14, 15] for the benefits of this projection for highly heterogeneous media). We note that slope limiters are not used in our proposed algorithm as they are not needed for stability. The choice of primary variables and the formulation of the model problem produce an algorithm that easily handles the appearance and disappearance of phases without additional effort.

DG methods have been applied successfully for simulating incompressible two-phase flows without mass transfer over the last decade. The use of discontinuous elements allows for a flexible method that can handle unstructured grids, full matrix coefficients and that produces numerical solutions with artificial diffusion that is significantly less than in the case of cell-centered finite volume methods. There is an abundant literature on the topic where DG are used with other methods such as mixed finite element methods or where they are used stand-alone [16–22]. The DG literature for compositional flows (with mass transfer) is very sparse. For one-dimensional problems, we can mention the works [23, 24] where DG methods are used to solve the two-component two-phase flow problem of CO_2 sequestration problem using either linear relationship between pressure and density or nonlinear relationships. In [25], the black-oil problem in one-dimensional problems has been numerically discretized by high order DG methods (with polynomials of degree up to four), where mass transfer between the liquid and vapor phases is modeled by the gas–oil ratio.

Developing flexible numerical methods for solving multi-component multi-phase flows with mass transfer is an active and rich area of research. In addition to DG methods, mixed hybrid finite element (MHFE) methods and multi-point flux approximation (MPFA) discretizations are locally mass conservative numerical methods that can handle complex grids and full matrix coefficients [26, 27]. In [28], MHFE methods for pressure and DG for explicit mass transport update are used for compositional three-phase flows without capillary pressure. In [29], multi-point flux mixed methods are introduced for a sequential implicit formulation of the compositional equations. We propose to use DG methods because they easily allow for the implementation of high order (global or local) polynomial approximation and local mesh adaptivity. While these attractive features are not the object of this paper, they form additional motivation for the use of DG methods.

The paper is organized as follows. Section 2 presents the mathematical equations describing the black oil problem. The time discretization of our algorithm, based on the formulations of [12, 30] is introduced in Section 3. Section 4 describes the full discretization of our method using DG finite elements. The convergence properties of this approximation method are studied with manufactured solutions in Section 5. Problems involving gravity effects, mass transfer and phase disappearance, are solved in Sections 6 and 7, respectively. Finally, we show the robustness of our scheme in Section 8 by studying a gas–water injection problem in a highly heterogeneous media.

2 | BLACK OIL MODEL

This section introduces the variables and the equations involved in a black oil problem with three components (oil, gas, water) and three phases (liquid, vapor, aqueous) in a porous medium Ω. We assume that the oil and gas components may exist in the liquid and vapor phases, and that the aqueous phase is uniquely formed of water. The notation used in this section is classical for multiphase flows in porous media [2].

2.1 | Notation and set-up

We introduce the fraction of oil in the liquid phase $x_{o,\ell}$ and the fraction of gas in liquid phase $x_{g,\ell}$. They are defined as follows:

$$x_{o,\ell} = \frac{\text{mass oil in liquid}}{\text{mass liquid}}, \qquad x_{g,\ell} = \frac{\text{mass gas in liquid}}{\text{mass liquid}}.$$

The liquid is exclusively composed of oil and gas, so these fractions satisfy the following equality:

$$x_{o,\ell} + x_{g,\ell} = 1. \tag{2.1}$$

We also introduce the fraction of oil in the vapor phase $x_{o,v}$, respectively the fraction of gas in vapor phase $x_{g,v}$. They are defined as follows:

$$x_{o,v} = \frac{\text{mass oil in vapor}}{\text{mass vapor}}, \qquad x_{g,v} = \frac{\text{mass gas in vapor}}{\text{mass vapor}}.$$

As the vapor is uniquely composed of oil and gas, these fractions satisfy the relation:

$$x_{o,v} + x_{g,v} = 1. \tag{2.2}$$

The aqueous phase is only composed of water so the fraction of water in aqueous phase $x_{w,a}$ is equal to 1. The saturations of the liquid phase, the vapor phase and the aqueous phases are denoted by S_ℓ, S_v and S_a. They are defined as follows:

$$S_\ell = \frac{\text{volume liquid phase}}{\text{volume pore}}, \qquad S_v = \frac{\text{volume vapor phase}}{\text{volume pore}}, \qquad S_a = \frac{\text{volume aqueous phase}}{\text{volume pore}},$$

and satisfy the equation:

$$S_l + S_v + S_a = 1. \tag{2.3}$$

In the following of this paper, we enforce that the mass fractions satisfies:

$$(x_{o,\ell}, x_{g,\ell}) = (1, 0) \text{ if } S_\ell = 0, \tag{2.4}$$

$$(x_{o,v}, x_{g,v}) = (0, 1) \text{ if } S_v = 0. \tag{2.5}$$

Moreover, we assume that:

$$x_{g,\ell} < x_{g,v}. \tag{2.6}$$

The purpose of hypothesis (2.4)–(2.5) is to give a definition to the mass fractions of a phase that is not present. Our choice, of setting $x_{o,\ell} = 1$ when the liquid phase disappears, is motivated by the fact that the gas component should turn into vapor faster than the oil component. Thus, before completly disappearing the liquid phase should only contain oil. The same argumentation is used to set $x_{g,v} = 1$ when $S_v = 0$. Hypothesis (2.6) is required to prove that the algorithm introduced in Section 3 gives rise to a unique set of saturations (S_ℓ, S_v, S_a). A physical interpretation of this condition is that the gas component is always more represented in the vapor phase. Such condition is consistent with the above hypothesis when there is no vapor phase.

2.2 | Black oil problem equations

A black oil problem consists of approximating the solution of the mass conservation of the gas, oil and water components under the assumptions (2.1)–(2.3). The mass conservation equations of the oil, gas and water components are expressed as follows:

$$\partial_t(\phi(x_{o,\ell}\rho_\ell S_\ell + x_{o,v}\rho_v S_v)) - \nabla\cdot(x_{o,\ell}\rho_\ell\lambda_\ell(\nabla p_\ell - \rho_\ell\mathbf{g}) + x_{o,v}\rho_v\lambda_v(\nabla p_v - \rho_v\mathbf{g})) = x_{o,\ell}\rho_\ell q_\ell + x_{o,v}\rho_v q_v, \tag{2.7}$$

$$\partial_t(\phi(x_{g,\ell}\rho_\ell S_\ell + x_{g,v}\rho_v S_v)) - \nabla\cdot(x_{g,\ell}\rho_\ell\lambda_\ell(\nabla p_\ell - \rho_\ell\mathbf{g}) + x_{g,v}\rho_v\lambda_v(\nabla p_v - \rho_v\mathbf{g})) = x_{g,\ell}\rho_\ell q_\ell + x_{g,v}\rho_v q_v, \tag{2.8}$$

$$\partial_t(\phi\rho_a S_a) - \nabla\cdot(\rho_a\lambda_a(\nabla p_a - \rho_a\mathbf{g})) = \rho_a q_a, \tag{2.9}$$

where p_ℓ is the pressure of the liquid phase, p_v is the pressure of the vapor phase and p_a is the pressure of the aqueous phase. The function ϕ is the porosity and the coefficients ρ_ℓ, ρ_v and ρ_a are the phases densities. The phase mobilities are denoted by λ_ℓ, λ_v and λ_a. We recall that λ_j is defined as the ratio $\kappa_{\text{abs}}\kappa_j/\mu_j$ where κ_{abs} is the absolute permeability, μ_j is the viscosity that only depends of the pressure p_j and κ_j is the relative permeability that only depends of the saturation S_j. The gravity is denoted by $\mathbf{g}$ and the functions q_ℓ, q_v and q_a are source/sink terms. In the rest of the paper, we assume that

$$\rho_v \leq \rho_\ell. \tag{2.10}$$

This condition is used in Section 3.2.5 to prove that a unique set of saturations (S_ℓ, S_v) is derived from our formulation.

2.3 | Introduction of capillary pressures and reformulation of black oil problem

The action of capillary effects induces a difference in pressure between the three phases. Although the quantities p_ℓ, p_v and p_a differ, they are linked to each other by the capillary pressures $p_{c,v}$ and $p_{c,a}$ defined as follows:

$$p_{c,v} = p_v - p_\ell, \qquad p_{c,a} = p_\ell - p_a. \tag{2.11}$$

The function $p_{c,v}$, respectively $p_{c,a}$, is assumed to uniquely depend of the variable S_v, respectively of S_v and S_a. Thus, we can write:

$$p_{c,v} = p_{c,v}(S_v), \qquad p_{c,a} = p_{c,a}(S_v, S_a). \tag{2.12}$$

Moreover the capillary pressures are assumed to be differentiable functions of S_v and S_a. The introduction of $p_{c,v}$ and $p_{c,a}$ allows us to eliminate the variables p_v and p_a from Equations (2.7)–(2.9). We note that the component mass fractions, phases densities and porosity are function of the phases pressures. Furthermore, the phases mobilities are function of the phases saturations. Thus, one can

show that approximating the solutions of a black oil problem can be reduced to approximating the liquid pressure and the aqueous and vapor phase saturations.

3 | ALGORITHM FOR DISCRETIZATION IN TIME

We present a new time stepping algorithm to approximate Equations (2.7)–(2.9) inspired from [12, 30]. This algorithm is consistent with the three-phase black oil model described in Section 2. In the remainder of the paper, we let $\tau > 0$ be a time step and $n \geq 0$ an integer. A function f evaluated at the time $n\tau$ is denoted by f^n.

3.1 | Strategy and introduction of new variable

To approximate the black oil problem (2.7)–(2.9) we choose the aqueous saturation S_a as independent primary variable. In the wake of Shank and Vestal [12], Hajibeygi and Tchelepi [30], we choose the liquid pressure and the total fraction of gas in the media, denoted by z_g, as the remaining two independent primary variables. The liquid pressure is approximated as the solution of the sum of the three mass conservation Equations (2.7)–(2.9). It reads p_ℓ solution of:

$$\begin{aligned}&\partial_t(\phi(\rho_\ell S_\ell + \rho_v S_v + \rho_a S_a)) - \nabla \cdot (\rho_\ell \lambda_\ell(\nabla p_\ell - \rho_\ell \mathbf{g})) - \nabla \cdot (\rho_v \lambda_v(\nabla p_v - \rho_v \mathbf{g}))\\ &\quad - \nabla \cdot (\rho_a \lambda_a(\nabla p_a - \rho_a \mathbf{g})) = \rho_\ell q_\ell + \rho_v q_v + \rho_a q_a,\end{aligned} \tag{3.1}$$

where p_v and p_a can be substituted with p_ℓ and the capillary pressures $p_{c,v}$ and $p_{c,a}$ defined by (2.11). The total fraction of gas in the media z_g is defined as follows:

$$z_g = x_{g,\ell} \frac{\rho_\ell S_\ell}{\rho_\ell S_\ell + \rho_v S_v + \rho_a S_a} + x_{g,v} \frac{\rho_v S_v}{\rho_\ell S_\ell + \rho_v S_v + \rho_a S_a}. \tag{3.2}$$

We note that z_g is a convex combination of $(x_{g,\ell}, x_{g,v}, 0)$. The assumption (2.6) implies that $0 \leq z_g \leq x_{g,v}$. Using the definition of the capillary pressure $p_{c,v}$, the mass conservation of the gas component can be rewritten in function of z_g. It reads z_g solution of the following equation:

$$\partial_t(\phi \rho_t z_g) - \nabla \cdot (F_g(\rho\lambda)_t \nabla p_\ell) - \nabla \cdot (x_{g,v} \lambda_v \rho_v \nabla p_{c,v}) + \nabla \cdot ((x_{g,\ell} \rho_\ell^2 \lambda_\ell + x_{g,\ell} \rho_v^2 \lambda_v)\mathbf{g}) = f_g(\rho q)_t, \tag{3.3}$$

where

$$\rho_t = \rho_\ell S_\ell + \rho_v S_v + \rho_a S_a, \qquad (\rho\lambda)_t = \rho_\ell \lambda_\ell + \rho_v \lambda_v + \rho_a \lambda_a, \qquad (\rho q)_t = \rho_\ell q_\ell + \rho_v q_v + \rho_a q_a.$$

This formulation also involves the gas fractional flow $F_g = x_{g,\ell} F_{g,\ell} + x_{g,v} F_{g,v}$ with the following phases fractional flows:

$$F_{g,\ell} = \frac{\rho_\ell \lambda_\ell}{\rho_\ell \lambda_\ell + \rho_v \lambda_v + \rho_a \lambda_a} \qquad \text{and} \qquad F_{g,v} = \frac{\rho_v \lambda_v}{\rho_\ell \lambda_\ell + \rho_v \lambda_v + \rho_a \lambda_a}.$$

The source term f_g is equal to $x_{g,\ell} f_{g,\ell} + x_{g,v} f_{g,v}$ where the liquid source term is $f_{g,\ell} = \frac{\rho_\ell q_\ell}{(\rho q)_t}$ and the vapor source term is $f_{g,v} = \frac{\rho_v q_v}{(\rho q)_t}$.

We conclude this section with boundary conditions for the three primary variables. The boundary of the domain is decomposed as follows:

$$\partial\Omega = \Gamma_D^p \cup \Gamma_N^p = \Gamma_D^S \cup \Gamma_N^S = \Gamma_D^z \cup \Gamma_N^z.$$

Dirichlet boundary conditions are imposed on Γ_D^p for the liquid pressure, respectively on Γ_D^S and Γ_D^z for the aqueous saturation and the variable z_g. The boundary conditions imposed on these surfaces

are denoted by p_ℓ^{bdy}, S_a^{bdy} and z_g^{bdy}. Neumann boundary conditions are imposed on Γ_N^p for the liquid pressure, respectively on Γ_N^S and Γ_N^z for the aqueous saturation and the variable z_g as described below:

$$(\rho\lambda)_t \nabla p_\ell \cdot \mathbf{n} = j_p^{\text{N}}, \qquad \rho_a \lambda_a \frac{\partial p_{c,a}}{\partial S_a} \nabla S_a \cdot \mathbf{n} = j_S^{\text{N}}, \qquad x_{g,v} \rho_v \lambda_v \frac{\partial p_{c,v}}{\partial S_v} \frac{\partial S_v}{\partial z_g} \nabla z_g \cdot \mathbf{n} = j_z^{\text{N}}.$$

3.2 | Time marching

After an initialization step of the variables introduced in the previous sections, the algorithm proceeds as follows.

3.2.1 | Liquid pressure

The liquid pressure is updated as the solution of the sum of the mass conservation Equations (3.1). Using a backward difference formula of order one to discretize the time derivative, first order extrapolation of fluid–vapor–aqueous phases properties and the definition of the capillary pressures (2.11), gives p_ℓ^{n+1} solution of the following equation:

$$\begin{aligned} &\frac{\phi^n \rho_t^n - \phi^{n-1} \rho_t^{n-1}}{\tau} - \nabla \cdot ((\rho\lambda)_t^n \nabla p_\ell^{n+1}) - \nabla \cdot (\rho_v^n \lambda_v^n \nabla p_{c,v}^n) + \nabla \cdot (\rho_a^n \lambda_a^n \nabla p_{c,a}^n) \\ &\quad = (\rho q)_t^{*,n+1} - \nabla \cdot (((\rho_\ell^2)^n \lambda_\ell^n + (\rho_v^2)^n \lambda_v^n + (\rho_a^2)^n \lambda_a^n)\mathbf{g}), \end{aligned} \tag{3.4}$$

where

$$(\rho q)_t^{*,n+1} = \rho_\ell^n q_\ell^{n+1} + \rho_v^n q_v^{n+1} + \rho_a^n q_a^{n+1}.$$

The vapor and aqueous pressures are then updated using (2.11) as follows:

$$p_v^{n+1} = p_\ell^{n+1} + p_{c,v}^n, \qquad p_a^{n+1} = p_\ell^{n+1} - p_{c,a}^n. \tag{3.5}$$

Remark 3.1 We can now compute the components fractions $x_{o,\ell}^{n+1}$, $x_{o,v}^{n+1}$, $x_{g,\ell}^{n+1}$, $x_{g,v}^{n+1}$ and the phases densities ρ_ℓ^{n+1}, ρ_v^{n+1}, ρ_a^{n+1} using p_ℓ^{n+1}, p_v^{n+1} and p_a^{n+1}.

3.2.2 | Aqueous saturation

The aqueous saturation is the solution of the water component conservation equation. Using Equation (2.11), it gives S_a solution of:

$$\partial_t(\rho_a S_a) + \nabla \cdot (\rho_a \lambda_a \nabla p_{c,a}) = \nabla \cdot (\rho_a \lambda_a (\nabla p_\ell - \rho_a \mathbf{g})) + \rho_a q_a. \tag{3.6}$$

As the capillary pressure $p_{c,a}$ is a differentiable function of S_v and S_a, and only depends of these variables, one can write:

$$\nabla p_{c,a} = \frac{\partial p_{c,a}}{\partial S_v} \nabla S_v + \frac{\partial p_{c,a}}{\partial S_a} \nabla S_a. \tag{3.7}$$

Eventually, we solve S_a^{n+1} solution of the following equation:

$$\begin{aligned} &\frac{\phi^{n+1} \rho_a^{n+1} S_a^{n+1} - \phi^n \rho_a^n S_a^n}{\tau} + \nabla \cdot \left(\rho_a^{n+1} \lambda_a^n \left(\frac{\partial p_{c,a}}{\partial S_a} \right)^n \nabla S_a^{n+1} \right) = \rho_a^{n+1} q_a^{n+1} \\ &\quad -\nabla \cdot \left(\rho_a^{n+1} \lambda_a^n \left(\frac{\partial p_{c,a}}{\partial S_v} \right)^n \nabla S_v^n \right) + \nabla \cdot (\rho_a^{n+1} \lambda_a^n (\nabla p_\ell^{n+1} - \rho_a^{n+1} \mathbf{g})), \end{aligned} \tag{3.8}$$

where we use a backward difference formula of order one to approximate the time derivative.

Remark 3.2 We can now compute the phases mobility λ_a^{n+1} using the saturations S_a^{n+1}. Moreover, since $\frac{\partial p_{c,a}}{\partial S_a}$ is negative by construction, the second term of the above left-hand side is a diffusive term.

3.2.3 | Total gas fraction

Before describing the scheme used to update z_g, we note that the saturation S_v is a differentiable function of z_g, $x_{g,\ell}$, $x_{g,v}$, S_a, ρ_ℓ, ρ_v, and ρ_a (see Section 3.2.5).

As the capillary pressure $p_{c,v}$ is a differentiable function of S_v, the term $\nabla p_{c,v}$ can be rewritten as follows:

$$\nabla p_{c,v} = \frac{\partial p_{c,v}}{\partial S_v}\left(\frac{\partial S_v}{\partial z_g}\nabla z_g + \frac{\partial S_v}{\partial x_{g,\ell}}\nabla x_{g,\ell} + \frac{\partial S_v}{\partial x_{g,v}}\nabla x_{g,v} + \frac{\partial S_v}{\partial S_a}\nabla S_a + \frac{\partial S_v}{\partial \rho_\ell}\nabla \rho_\ell + \frac{\partial S_v}{\partial \rho_v}\nabla \rho_v + \frac{\partial S_v}{\partial \rho_a}\nabla \rho_a\right). \tag{3.9}$$

The variable z_g^{n+1} is computed as the solution of the following problem:

$$\begin{aligned}
&\frac{\phi\rho_t^{*,n+1}z_g^{n+1}}{\tau} - \nabla\cdot\left(\left(\frac{\partial F_g}{\partial z_g}\right)^n z_g^{n+1}(\rho\lambda)_t^{*,n+1}\nabla p_\ell^{n+1}\right) - \nabla\cdot\left(x_{g,v}^{n+1}\rho_v^{n+1}\lambda_v^n\left(\frac{\partial p_{c,v}}{\partial S_v}\right)^n\left(\frac{\partial S_v}{\partial z_g}\right)^{+,n}\nabla z_g^{n+1}\right)\\
&\quad= \frac{\phi\rho_t^{*,n}z_g^n}{\tau} + f_g^{n+1}(\rho q)_t^{n+1} + \nabla\cdot\left(\left(F_g^n - \left(\frac{\partial F_g}{\partial z_g}\right)^n z_g^n\right)(\rho\lambda)_t^{*,n+1}\nabla p_\ell^{n+1}\right)\\
&\qquad+\nabla\cdot\left(x_{g,v}^{n+1}\rho_v^{n+1}\lambda_v^n\left(\frac{\partial p_{c,v}}{\partial S_v}\right)^n\left(\left(\frac{\partial S_v}{\partial z_g}\right)^{-,n}\nabla z_g^n + \left(\frac{\partial S_v}{\partial x_{g,\ell}}\right)^n\nabla x_{g,\ell}^{n+1} + \left(\frac{\partial S_v}{\partial x_{g,v}}\right)^n\nabla x_{g,v}^{n+1}\right)\right)\\
&\qquad+\nabla\cdot\left(x_{g,v}^{n+1}\rho_v^{n+1}\lambda_v^n\left(\frac{\partial p_{c,v}}{\partial S_v}\right)^n\left(\left(\frac{\partial S_v}{\partial S_a}\right)^n\nabla S_a^{n+1}\right.\right.\\
&\qquad\left.\left.+\left(\frac{\partial S_v}{\partial \rho_\ell}\right)^n\nabla\rho_\ell^{n+1} + \left(\frac{\partial S_v}{\partial \rho_v}\right)^n\nabla\rho_v^{n+1} + \left(\frac{\partial S_v}{\partial \rho_a}\right)^n\nabla\rho_a^{n+1}\right)\right)\\
&\qquad-\nabla\cdot((x_{g,\ell}^{n+1}(\rho_\ell^2)^{n+1}\lambda_\ell^n + x_{g,v}^{n+1}(\rho_v^{n+1})^2\lambda_v^n)\mathbf{g}),
\end{aligned} \tag{3.10}$$

where we set

$$\rho_t^{*,n+1} = \rho_\ell^{n+1}S_\ell^n + \rho_v^{n+1}S_v^n + \rho_a^{n+1}S_a^n, \qquad (\rho\lambda)_t^{*,n+1} = \rho_\ell^{n+1}\lambda_\ell^n + \rho_v^{n+1}\lambda_v^n + \rho_a^{n+1}\lambda_a^n.$$

We also split the term $\frac{\partial S_v}{\partial z_g}$ into its positive and negative parts. For any function f, we denote:

$$f^+ = \max(0,f), \qquad f^- = \min(0,f).$$

We use a backward difference formula of order one to approximate the time derivative and the following Taylor expansion: $F_g^{n+1} = F_g^n + \left(\frac{\partial F_g}{\partial z_g}\right)^n(z_g^{n+1} - z_g^n)$ where $\left(\frac{\partial F_g}{\partial z_g}\right)^n = \frac{\partial F_g}{\partial z_g}(z_g^n)$.

Remark 3.3 We note that $\frac{\partial p_{c,v}}{\partial S_v}$ is strictly positive. Thus, the term $\frac{\partial p_{c,v}}{\partial S_v}\left(\frac{\partial S_v}{\partial z_g}\right)^+$ is positive. We treat implicitly the diffusive part of the Laplace operator while the other part, involving the term $\left(\frac{\partial S_v}{\partial z_g}\right)^-$, is treated explicitly for stability purpose. We refer to the annex Appendix B for more details on the computation of the terms $\frac{\partial F_g}{\partial z_g}$, $\left(\frac{\partial S_v}{\partial z_g}\right)^+$, and $\left(\frac{\partial S_v}{\partial z_g}\right)^-$.

3.2.4 | Correction of the components fractions

We recall that the densities and $x_{g,v}$ are strictly positive, see hypothesis (2.6). Thus in the region where S_a is strictly positive, the variable z_g is zero if and only if S_v and $x_{g,\ell}S_\ell$ are zero. The condition S_ℓ equal

to zero implies that $x_{o,\ell}$ equal one and $x_{g,\ell}$ equal zero while the condition $x_{g,\ell}$ equal zero implies that $x_{o,\ell}$ is one. Similarly the condition S_v equal to zero implies that $(x_{g,v}, x_{o,v}) = (1, 0)$. As a consequence, we enforce $(x_{o,\ell}, x_{g,\ell}) = (1, 0)$ and $(x_{o,v}, x_{g,v}) = (0, 1)$ in the regions where S_a is strictly positive and z_g is zero. In the region where S_a is zero, the maximum value of $x_{g,\ell}$ is z_g. Thus, if the computed value of z_g is found to be smaller than $x_{g,\ell}$, we set $x_{g,\ell} = z_g$. In this case, we have S_v equal to zero so we can set $x_{g,v}$ to one.

3.2.5 | Liquid and vapor saturations

Using the definition of z_g and Equation (2.3), we have $(S_v^{n+1}, S_\ell^{n+1})$ solution of the following problem:

$$(z_g^{n+1} - x_{g,\ell}^{n+1})\rho_\ell^{n+1} S_\ell^{n+1} + (z_g^{n+1} - x_{g,v}^{n+1})\rho_v^{n+1} S_v^{n+1} = -z_g^{n+1}\rho_a^{n+1} S_a^{n+1}, \tag{3.11a}$$

$$S_\ell^{n+1} + S_v^{n+1} = 1 - S_a^{n+1}. \tag{3.11b}$$

The determinant of the above system is denoted by d and depends on z_g:

$$d(z_g) = (z_g - x_{g,\ell})\rho_\ell + (x_{g,v} - z_g)\rho_v. \tag{3.12}$$

As $d'(z_g)$ is equal to $\rho_\ell - \rho_v$, a positive term thanks to the hypothesis (2.10), the determinant of the above system is an increasing function of z_g. The variable z_g belongs to the interval $[0, x_{g,v}]$ so showing that $d(0)$ is strictly positive would imply that the above system has a unique solution. As shown in the previous section, z_g equal to zero implies that $(x_{g,\ell}, x_{g,v}) = (0, 1)$. Therefore, $d(0) = \rho_v$ is strictly positive and the above system has a unique solution defined by:

$$S_\ell^{n+1} = \frac{(x_{g,v}^{n+1} - z_g^{n+1})\rho_v^{n+1}(1 - S_a^{n+1}) - z_g^{n+1}\rho_a^{n+1} S_a^{n+1}}{(x_{g,v}^{n+1} - z_g^{n+1})\rho_v^{n+1} + (z_g^{n+1} - x_{g,\ell}^{n+1})\rho_\ell^{n+1}}, \tag{3.13}$$

$$S_v^{n+1} = \frac{(z_g^{n+1} - x_{g,\ell}^{n+1})\rho_\ell^{n+1}(1 - S_a^{n+1}) + z_g^{n+1}\rho_a^{n+1} S_a^{n+1}}{(x_{g,v}^{n+1} - z_g^{n+1})\rho_v^{n+1} + (z_g^{n+1} - x_{g,\ell}^{n+1})\rho_\ell^{n+1}}. \tag{3.14}$$

Remark 3.4 We can now compute the phases mobilities λ_ℓ^{n+1}, λ_v^{n+1} and the capillary pressures $p_{c,v}^{n+1}, p_{c,a}^{n+1}$ using the saturations S_ℓ^{n+1}, S_v^{n+1} and S_a^{n+1}.

3.3 | Subiteration scheme

In practice, at each time step, we iterate over the equations and approximate the variables $(p_\ell^{n+1}, S_a^{n+1}, z_g^{n+1})$ as follows.

- Set $k = 0$ and introduce p_ℓ^k, S_a^k and z_g^k equal to (p_ℓ^n, S_a^n, z_g^n). Similarly, we introduce densities, mass fractions, viscosities and relative permeabilities at iteration k.
- Solve p_ℓ^{k+1} solution of:

$$\begin{aligned}&\frac{\partial_{p_\ell}(\phi^k\rho_t^k)(p_\ell^{k+1} - p_\ell^k)}{\tau} + \frac{\phi^k\rho_t^k - \phi^n\rho_t^n}{\tau} - \nabla\cdot((\rho\lambda)_t^k\nabla p_\ell^{k+1})\\ &\quad - \nabla\cdot(\rho_v^k\lambda_v^k\nabla p_{c,v}^n) + \nabla\cdot(\rho_a^k\lambda_a^k\nabla p_{c,a}^n) + \nabla\cdot(((\rho_\ell^2)^k\lambda_\ell^k + (\rho_v^2)^k\lambda_v^k + (\rho_a^2)^k\lambda_a^k)\mathbf{g}) = (\rho q)_t^{*,k+1},\end{aligned}$$

where $(\rho q)_t^{*,k+1} = \rho_\ell^k q_\ell^{k+1} + \rho_v^k q_v^{k+1} + \rho_a^k q_a^{k+1}$. The time derivative is approximated with a backward difference formula of order one where the term $\phi^{k+1}\rho_t^{k+1}$ is approximated with a Taylor expansion of order one.

- Update the mass fractions and densities with p_ℓ^{k+1}.
- Solve S_a^{k+1} solution of:

$$\frac{\phi^k \rho_a^k S_a^{k+1} - \phi^n \rho_a^n S_a^n}{\tau} + \nabla \cdot \left(\rho_a^{k+1} \lambda_a^k \left(\frac{\partial p_{c,a}}{\partial S_a} \right)^k \nabla S_a^{k+1} \right) = \rho_a^{k+1} q_a^{n+1}$$
$$-\nabla \cdot \left(\rho_a^{k+1} \lambda_a^k \left(\frac{\partial p_{c,a}}{\partial S_v} \right)^k \nabla S_v^k \right) + \nabla \cdot (\rho_a^{k+1} \lambda_a^k (\nabla p_\ell^{k+1} - \rho_a^{k+1} \mathbf{g})),$$

- Update the relative permeability and viscosity of the aqueous phase.
- Solve z_g^{k+1} solution of:

$$\begin{aligned}
&\frac{\phi^{k+1} \rho_t^{*,k+1} z_g^{k+1}}{\tau} - \nabla \cdot \left(\left(\frac{\partial F_g}{\partial z_g} \right)^k z_g^{k+1} (\rho\lambda)_t^{*,k+1} \nabla p_\ell^{k+1} \right) - \nabla \cdot \left(x_{g,v}^{k+1} \rho_v^{k+1} \lambda_v^k \left(\frac{\partial p_{c,v}}{\partial S_v} \right)^k \left(\frac{\partial S_v}{\partial z_g} \right)^{+,k} \nabla z_g^{k+1} \right) \\
&= \frac{\phi^n \rho_t^{*,n} z_g^n}{\tau} + f_g^{n+1} (\rho q)_t^{n+1} + \nabla \cdot \left(\left(F_g^k - \left(\frac{\partial F_g}{\partial z_g} \right)^k z_g^k \right) (\rho\lambda)_t^{*,k+1} \nabla p_\ell^{k+1} \right) \\
&\quad + \nabla \cdot \left(x_{g,v}^{k+1} \rho_v^{k+1} \lambda_v^k \left(\frac{\partial p_{c,v}}{\partial S_v} \right)^k \left(\left(\frac{\partial S_v}{\partial z_g} \right)^{-,k} \nabla z_g^k + \left(\frac{\partial S_v}{\partial x_{g,\ell}} \right)^k \nabla x_{g,\ell}^{k+1} + \left(\frac{\partial S_v}{\partial x_{g,v}} \right)^k \nabla x_{g,v}^{k+1} \right) \right) \\
&\quad + \nabla \cdot \left(x_{g,v}^{k+1} \rho_v^{k+1} \lambda_v^k \left(\frac{\partial p_{c,v}}{\partial S_v} \right)^k \left(\left(\frac{\partial S_v}{\partial S_a} \right)^n \nabla S_a^{k+1} \right. \right. \\
&\quad \left. \left. + \left(\frac{\partial S_v}{\partial \rho_\ell} \right)^n \nabla \rho_\ell^{k+1} + \left(\frac{\partial S_v}{\partial \rho_v} \right)^n \nabla \rho_v^{k+1} + \left(\frac{\partial S_v}{\partial \rho_a} \right)^n \nabla \rho_a^{k+1} \right) \right) \\
&\quad - \nabla \cdot ((x_{g,\ell}^{k+1} (\rho_\ell^2)^{k+1} \lambda_\ell^k + x_{g,v}^{k+1} (\rho_v^{k+1})^2 \lambda_v^k) \mathbf{g}),
\end{aligned}$$

where $(\rho\lambda)_t^{*,k+1} = \rho_\ell^{k+1} \lambda_\ell^k + \rho_v^{k+1} \lambda_v^k + \rho_a^{k+1} \lambda_a^k$.

- Update the viscosities, relative permeabilities and saturations of the liquid and vapor phases.
- Compute the L^2 norm of $p_\ell^{k+1} - p_\ell^k$, $s_a^{k+1} - s_a^k$ and $z_g^{k+1} - z_g^k$.
- If the above norms are smaller than a given tolerance, set by the user, all the variables and fluid properties at time t_{n+1} are updated using the values at iteration $k+1$.
- Else, variables and fluid properties at iteration k are updated with their values at iteration $k+1$ and the above process is repeated.

As mentioned in Section 1, one can notice that the algorithm is independent of phase appearance and disappearance effects, since liquid and vapor phase saturations are not primary variables.

4 | FULL DISCRETIZATION WITH DISCONTINUOUS GALERKIN FINITE ELEMENT

We describe the spatial discretization, using DG finite element, of the algorithm introduced in Section 3. The weak formulation presented here is consistent with the subiteration scheme of Section 3.3.

4.1 | Domain discretization

Let $\mathcal{E}_h$ be a conforming mesh of the domain Ω where the mesh size is denoted by h. Let Γ_h be the set of all interior faces. The diameter of each face e is denoted by h_e. To each face $e \in \Gamma_h$, we associate a normal vector $\mathbf{n}_e$.

In the following, we also use the operator $\{\cdot\}$ defined as the weighted average of a function on an interior face and the operator $[\cdot]$ defined as the difference between the traces of a function from the neighboring elements of an interior face. The weights involved in the average operator $\{\cdot\}$ are computed with the formula introduced in Ern and coworkers [13]. For completeness, we recall the formula of the weighted average for a diffusion term of the form $-\nabla\cdot(A\nabla f)$ with A a scalar. Let e be an interior face. We denote by A_i, A_o, respectively ∇f_i and ∇f_o, the values of A, respectively ∇f, on the inner and outer interface of e. The weighted average formula reads:

$$\{A\nabla f\cdot\mathbf{n}_e\} = \omega_i A_i\nabla f_i\cdot\mathbf{n}_e + \omega_o A_o\nabla f_o\cdot\mathbf{n}_e, \tag{4.1}$$

where the weighted average ω_i and ω_o are defined as follows:

$$\omega_i = \frac{A_o}{A_iA_o}, \qquad \omega_o = \frac{A_i}{A_iA_o}. \tag{4.2}$$

In our scheme below, we apply this weighted average to diffusion-like terms and the diffusion coefficient depends on physical properties such as densities, relative permeabilities and so on.

4.2 | Approximation spaces

The liquid pressure, aqueous saturation and variable z_g are approximated in the following discontinuous finite element space:

$$X_h = \{v; v_{|K}\in\mathbb{P}_1(K), \forall K\in\mathcal{E}_h\}, \tag{4.3}$$

with the piecewise Lagrange function as basis function of the DG finite element space. The total Darcy velocity, defined by $\mathbf{u}_t = -(\rho\lambda)_t\nabla p_\ell$, and the aqueous velocity, defined by $\mathbf{u}_a = -\kappa_{\text{abs}}\nabla p_\ell$, are projected on the Raviart–Thomas space $\mathbb{RT}_0$ [31]. These projected velocities are used in the approximation of the variables S_a and z_g as described in the Sections 4.4 and 4.5. We refer to [14] for details on the projection method on these finite element spaces.

4.3 | Liquid pressure weak formulation

The liquid pressure p_ℓ^{k+1} is the solution of the following weak formulation for all $\phi\in X_h$:

$$\frac{1}{\tau}A_{p_\ell}^{\text{time}}(p_\ell^{k+1},\phi) + A_{p_\ell}^{\text{vol}}(p_\ell^{k+1},\phi) + A_{p_\ell}^{\text{bdy}}(p_\ell^{k+1},\phi) + A_{p_\ell}^{\text{int}}(p_\ell^{k+1},\phi) = 0, \tag{4.4}$$

where $A_{p_\ell}^{\text{time}}$ is the term associated to the time derivative, $A_{p_\ell}^{\text{vol}}$ represents the other volume terms, $A_{p_\ell}^{\text{bdy}}$ the boundaries terms and $A_{p_\ell}^{\text{int}}$ the interface terms of the liquid pressure weak formulation. They are defined as follows:

$$A_{p_\ell}^{\text{time}}(p_\ell^{k+1},\phi) = \sum_{K\in\mathcal{E}_h}\int_K(\partial_{p_\ell}(\phi^k\rho_t^k)(p_\ell^{k+1}-p_\ell^k) + \phi^k\rho_t^k - \phi^n\rho_t^n)\phi, \tag{4.5}$$

$$\begin{aligned} A_{p_\ell}^{\text{vol}}(p_\ell^{k+1},\phi) = &-\sum_{K\in\mathcal{E}_h}\int_K(\rho q)_t^{*,k+1}\phi, + \sum_{K\in\mathcal{E}_h}\int_K(\rho\lambda)_t^k\nabla p_\ell^{k+1}\cdot\nabla\phi \\ &+ \sum_{K\in\mathcal{E}_h}\int_K(\rho_v^k\lambda_v^k\nabla p_{c,v}^k - \rho_a^k\lambda_a^k\nabla p_{c,a}^k - ((\rho_\ell^2)^k\lambda_\ell^k + (\rho_v^2)^k\lambda_v^k + (\rho_a^2)^k\lambda_a^k)\mathbf{g})\cdot\nabla\phi \end{aligned} \tag{4.6}$$

$$
\begin{aligned}
A^{\text{bdy}}_{p_\ell}(p^{k+1}_\ell,\phi) = &-\sum_{e\in\Gamma^p_D}\int_e(\rho\lambda)^k_t\nabla p^{k+1}_\ell\cdot\mathbf{n}_e\phi+\sum_{e\in\Gamma^p_D}\gamma_{p_\ell}h_e^{-1}\int_e(p^{k+1}_\ell-p^{\text{bdy},n+1}_\ell)\phi\\
&+\sum_{e\in\Gamma^p_D}\theta_{p_\ell}\int_e(\rho\lambda)^k_t\nabla\phi\cdot\mathbf{n}_e(p^{k+1}_\ell-p^{\text{bdy},n+1}_\ell)\\
&-\sum_{e\in\Gamma^p_D}\int_e\rho^k_v\lambda^k_v\nabla p^k_{c,v}\cdot\mathbf{n}_e\phi+\sum_{e\in\Gamma^p_D}\int_e\rho^k_a\lambda^k_a\nabla p^k_{c,a}\cdot\mathbf{n}_e\phi\\
&+\sum_{e\in\Gamma^p_D}\int_e((\rho^2_\ell)^k\lambda^k_\ell+(\rho^2_v)^k\lambda^k_v+(\rho^2_a)^k\lambda^k_a)\mathbf{g}\cdot\mathbf{n}_e\phi+\sum_{e\in\Gamma^p_N}\int_e j^{\text{N}}_p\phi,
\end{aligned}
\tag{4.7}
$$

$$
\begin{aligned}
A^{\text{int}}_{p_\ell}(p^{k+1}_\ell,\phi) = &-\sum_{e\in\Gamma_h}\int_e\{(\rho\lambda)^k_t\nabla p^{k+1}_\ell\cdot\mathbf{n}_e\}[\phi]+\sum_{e\in\Gamma_h}\gamma_{p_\ell}h_e^{-1}\int_e[p^{k+1}_\ell][\phi]\\
&+\sum_{e\in\Gamma_h}\theta_{p_\ell}\int_e\{(\rho\lambda)^k_t\nabla\phi\cdot\mathbf{n}_e\}[p^{k+1}_\ell]\\
&-\sum_{e\in\Gamma_h}\int_e\{\rho^k_v\lambda^k_v\nabla p^k_{c,v}\cdot\mathbf{n}_e\}[\phi]+\sum_{e\in\Gamma_h}\int_e\{\rho^k_a\lambda^k_a\nabla p^k_{c,a}\cdot\mathbf{n}_e\}[\phi]\\
&+\sum_{e\in\Gamma_h}\int_e\{((\rho^2_\ell)^k\lambda^k_\ell+(\rho^2_v)^k\lambda^k_v+(\rho^2_a)^k\lambda^k_a)\mathbf{g}\cdot\mathbf{n}_e\}[\phi].
\end{aligned}
\tag{4.8}
$$

The penalty parameter γ_{p_ℓ} is a positive number. The variable θ_{p_ℓ} is an integer equal to either -1 (Symmetric Interior Penalty Galerkin), 0 (Incomplete Interior Penalty Galerkin) or 1 (Nonsymmetric Interior Penalty Galerkin). It is set to zero in the following. The term $(\rho q)^{*,\,k+1}$ is computed with the densities at subiteration k and the source term at the time iteration $n+1$.

4.4 | Aqueous saturation weak formulation

The aqueous saturation S^{k+1}_a is the solution of the following formulation for all $\phi\in X_h$:

$$
\frac{1}{\tau}A^{\text{time}}_{S_a}(S^{k+1}_a,\phi)+A^{\text{vol}}_{S_a}(S^{k+1}_a,\phi)+A^{\text{bdy}}_{S_a}(S^{k+1}_a,\phi)+A^{\text{int}}_{S_a}(S^{k+1}_a,\phi)=0,
\tag{4.9}
$$

where $A^{\text{time}}_{S_a}$, $A^{\text{vol}}_{S_a}$, $A^{\text{bdy}}_{S_a}$ and $A^{\text{int}}_{S_a}$ are respectively the time derivative term, other volume terms, the boundaries terms and the interface terms of the aqueous saturations weak formulation. They are defined as follows:

$$
A^{\text{time}}_{S_a}(S^{k+1}_a,\phi)=\sum_{K\in\mathcal{E}_h}\int_K(\phi^{k+1}\rho^{k+1}_aS^{k+1}_a-\phi^n\rho^n_aS^n_a)\phi,
\tag{4.10}
$$

$$
\begin{aligned}
A^{\text{vol}}_{S_a}(S^{k+1}_a,\phi) = &-\sum_{K\in\mathcal{E}_h}\int_K\rho^{k+1}_a\lambda^k_a\left(\frac{\partial p_{c,a}}{\partial S_a}\right)^k\nabla S^{k+1}_a\cdot\nabla\phi-\sum_{K\in\mathcal{E}_h}\int_K\rho^{k+1}_a\lambda^k_a\left(\frac{\partial p_{c,a}}{\partial S_v}\right)^k\nabla S^k_v\cdot\nabla\phi\\
&-\sum_{K\in\mathcal{E}_h}\int_K\left(\rho^{k+1}_a\frac{\kappa^k_a}{\mu^k_a}\mathbf{u}^{k+1}_a+(\rho^{k+1}_a)^2\lambda^k_a\mathbf{g}\right)\cdot\nabla\phi-\sum_{K\in\mathcal{E}_h}\int_K\rho^{k+1}_aq^{n+1}_a\phi,
\end{aligned}
\tag{4.11}
$$

$$
\begin{aligned}
A^{\text{bdy}}_{S_a}(S^{k+1}_a,\phi) = &\sum_{e\in\Gamma^S_D}\int_e\rho^{k+1}_a\lambda^k_a\left(\frac{\partial p_{c,a}}{\partial S_a}\right)^k\nabla S^{k+1}_a\cdot\mathbf{n}_e\phi+\sum_{e\in\Gamma^S_D}\gamma_{S_a}h_e^{-1}\int_e(S^{k+1}_a-S^{\text{bdy},n+1}_a)\phi\\
&-\sum_{e\in\Gamma^S_D}\theta_{S_a}\int_e\rho^{k+1}_a\lambda^k_a\left(\frac{\partial p_{c,a}}{\partial S_a}\right)^k\nabla\phi\cdot\mathbf{n}_e(S^{k+1}_a-S^{\text{bdy},n+1}_a)
\end{aligned}
$$

$$
\begin{aligned}
&+ \sum_{e\in\Gamma_D^S}\int_e \rho_a^{k+1}\lambda_a^k\left(\frac{\partial p_{c,a}}{\partial S_v}\right)^k \nabla S_v^k\cdot\mathbf{n}_e\phi \\
&+ \sum_{e\in\Gamma_D^S}\int_e \left(\rho_a^{k+1}\frac{\kappa_a^k}{\mu_a^k}\mathbf{u}_a^{k+1} + (\rho_a^{k+1})^2\lambda_a^k\mathbf{g}\right)\cdot\mathbf{n}_e\phi + \sum_{e\in\Gamma_N^S}\int_e j_S^N\phi, \qquad (4.12)
\end{aligned}
$$

$$
\begin{aligned}
A_{S_a}^{\text{int}}(S_a^{k+1},\phi) = &\sum_{e\in\Gamma_h}\int_e \left\{\rho_a^{k+1}\lambda_a^k\left(\frac{\partial p_{c,a}}{\partial S_a}\right)^k \nabla S_a^{k+1}\cdot\mathbf{n}_e\right\}[\phi] + \sum_{e\in\Gamma_h}\gamma_{s_a}h_e^{-1}\int_e [S_a^{k+1}][\phi] \\
&- \sum_{e\in\Gamma_h}\theta_{S_a}\int_e \left\{\rho_a^{k+1}\lambda_a^k\left(\frac{\partial p_{c,a}}{\partial S_a}\right)^k \nabla\phi\cdot\mathbf{n}_e\right\}[S_a^{k+1}] \\
&+ \sum_{e\in\Gamma_h}\int_e \left\{\rho_a^{k+1}\lambda_a^k\left(\frac{\partial p_{c,a}}{\partial S_v}\right)^k \nabla S_v^k\cdot\mathbf{n}_e\right\}[\phi] \\
&+ \sum_{e\in\Gamma_h}\int_e \left\{\left(\rho_a^{k+1}\frac{\kappa_a^k}{\mu_a^k}\mathbf{u}_a^{k+1} + (\rho_a^{k+1})^2\lambda_a^k\mathbf{g}\right)\cdot\mathbf{n}_e\right\}[\phi], \qquad (4.13)
\end{aligned}
$$

where $\gamma_{s_a} > 0$ is a penalty parameter and $\mathbf{u}_a$ the projection of $\kappa_{\text{abs}}\nabla p_\ell^{k+1}$ on the Raviart–Thomas space $\mathbb{RT}_0$. The integer θ_{S_a} can be set to -1, 0, 1. In the rest of the paper, we set $\theta_{S_a} = 1$.

4.5 | Gas fraction z_g weak formulation

The variable z_g^{k+1} is the solution of the following formulation for all $\phi \in X_h$:

$$
\frac{1}{\tau}A_{z_g}^{\text{time}}(z_g^{k+1},\phi) + A_{z_g}^{\text{vol}}(z_g^{k+1},\phi) + A_{z_g}^{\text{bdy}}(z_g^{k+1},\phi) + A_{z_g}^{\text{int}}(z_g^{k+1},\phi) = 0, \qquad (4.14)
$$

with $A_{z_g}^{\text{time}}$, respectively $A_{z_g}^{\text{vol}}$, $A_{z_g}^{\text{bdy}}$ and $A_{z_g}^{\text{int}}$, the time derivative term, respectively the other volume terms, the boundaries and interface terms, of z_g weak formulation. They are defined by:

$$
A_{z_g}^{\text{time}}(z_g^{k+1},\phi) = \sum_{K\in\mathcal{E}_h}\int_K (\phi^{k+1}\rho_t^{*,k+1}z_g^{k+1} - \phi^n\rho_t^{*,n}z_g^n)\phi, \qquad (4.15)
$$

$$
\begin{aligned}
A_{z_g}^{\text{vol}}(z_g^{k+1},\phi) = &\sum_{K\in\mathcal{E}_h}\int_K x_{g,v}^{k+1}\rho_v^{k+1}\lambda_v^k\left(\frac{\partial p_{c,v}}{\partial S_v}\right)^k\left(\left(\frac{\partial S_v}{\partial z_g}\right)^{+,k}\nabla z_g^{k+1} + \left(\frac{\partial S_v}{\partial z_g}\right)^{-,k}\nabla z_g^k + \mathbf{A}_{S_v}^k\right)\cdot\nabla\phi \\
&- \sum_{K\in\mathcal{E}_h}\int_K \left(F_g^k + \left(\frac{\partial F_g}{\partial z_g}\right)^k(z_g^{k+1} - z_g^k)\right)\mathbf{u}_t^{*,k+1}\cdot\nabla\phi \\
&- \sum_{K\in\mathcal{E}_h}\int_K (x_{g,\ell}^{k+1}\rho_\ell^{k+1}q_\ell^{n+1} + x_{g,v}^{k+1}\rho_v^{k+1}q_v^{n+1})\phi \\
&- \sum_{K\in\mathcal{E}_h}\int_K (x_{g,\ell}^{k+1}(\rho_\ell^2)^{k+1}\lambda_\ell^k + x_{g,v}^{k+1}(\rho_v^{k+1})^2\lambda_v^k)\mathbf{g}\cdot\nabla\phi, \qquad (4.16)
\end{aligned}
$$

$$
\begin{aligned}
A_{z_g}^{\text{bdy}}(z_g^{k+1},\phi) = &-\sum_{e\in\Gamma_D^p}\int_e x_{g,v}^{k+1}\rho_v^{k+1}\lambda_v^k\left(\frac{\partial p_{c,v}}{\partial S_v}\right)^k\left(\left(\frac{\partial S_v}{\partial z_g}\right)^{+,k}\nabla z_g^{k+1} + \left(\frac{\partial S_v}{\partial z_g}\right)^{-,k}\nabla z_g^k + \mathbf{A}_{S_v}^k\right)\cdot\mathbf{n}_e\phi \\
&+ \sum_{e\in\Gamma_D^p}\int_e \left(F_g^k + \left(\frac{\partial F_g}{\partial z_g}\right)^k(z_g^{k+1} - z_g^k)\right)\mathbf{u}_t^{*,k+1}\cdot\mathbf{n}_e\phi
\end{aligned}
$$

$$+\sum_{e\in\Gamma_D^p}\int_e (x_{g,\ell}^{k+1}(\rho_\ell^2)^{k+1}\lambda_\ell^k + x_{g,v}^{k+1}(\rho_v^{k+1})^2\lambda_v^k)\mathbf{g}\cdot\mathbf{n}_e\phi + \sum_{e\in\Gamma_D^p}\gamma_{z_g}h_e^{-1}\int_e (z_g^{k+1}-z_g^{\mathrm{bdy},n+1})\phi$$

$$+\sum_{e\in\Gamma_D^p}\theta_{z_g}\int_e x_{g,v}^{k+1}\rho_v^{k+1}\lambda_v^k\left(\frac{\partial p_{c,v}}{\partial S_v}\right)^k\left(\frac{\partial S_v}{\partial z_g}\right)^{+,k}\nabla\phi\cdot\mathbf{n}_e z_g^{k+1} + \sum_{e\in\Gamma_N^Z}\int_e j_z^N\phi, \tag{4.17}$$

$$A_{z_g}^{\mathrm{int}}(z_g^{k+1},\phi) = -\sum_{e\in\Gamma_h}\int_e\left\{x_{g,v}^{k+1}\rho_v^{k+1}\lambda_v^k\left(\frac{\partial p_{c,v}}{\partial S_v}\right)^k\left(\left(\frac{\partial S_v}{\partial z_g}\right)^{+,k}\nabla z_g^{k+1} + \left(\frac{\partial S_v}{\partial z_g}\right)^{-,k}\nabla z_g^n + \mathbf{A}_{S_v}^k\right)\cdot\mathbf{n}_e\right\}[\phi]$$

$$+\sum_{e\in\Gamma_h}\gamma_{z_g}h_e^{-1}\int_e[z_g^{k+1}][\phi] + \sum_{e\in\Gamma_h}\theta_{z_g}\int_e\left\{x_{g,v}^{k+1}\rho_v^{k+1}\lambda_v^n\left(\frac{\partial p_{c,v}}{\partial S_v}\right)^k\left(\frac{\partial S_v}{\partial z_g}\right)^{+,k}\nabla\phi\cdot\mathbf{n}_e\right\}[z_g^{k+1}]$$

$$+\sum_{e\in\Gamma_h}\int_e\left\{\left(F_g^k+\left(\frac{\partial F_g}{\partial z_g}\right)^k(z_g^{k+1}-z_g^k)\right)\mathbf{u}_t^{*,k+1}\cdot\mathbf{n}_e\right\}^{\uparrow}[\phi]$$

$$+\sum_{e\in\Gamma_h}\int_e\{(x_{g,\ell}^{k+1}(\rho_\ell^2)^{k+1}\lambda_\ell^k + x_{g,v}^{k+1}(\rho_v^{k+1})^2\lambda_v^k)\mathbf{g}\cdot\mathbf{n}_e\}[\phi], \tag{4.18}$$

where $\gamma_{z_g} > 0$ is a penalty parameter, $\mathbf{u}_t^{*,k+1}$ is the projection of $-(\rho_\ell^{k+1}\lambda_\ell^k + \rho_v^{k+1}\lambda_v^k + \rho_a^{k+1}\lambda_a^k)\nabla p_\ell^{k+1}$ on the Raviart–Thomas space $\mathbb{RT}_0$ and θ_{z_g} an integer in $-1, 0, 1$. We set $\theta_{z_g} = 1$ in the following. The above weak formulation also introduces the variable $\mathbf{A}_{S_v}^k$ defined as follows:

$$\mathbf{A}_{S_v}^k = \left(\frac{\partial S_v}{\partial x_{g,\ell}}\right)^k\nabla x_{g,\ell}^{k+1} + \left(\frac{\partial S_v}{\partial x_{g,v}}\right)^k\nabla x_{g,v}^{k+1} + \left(\frac{\partial S_v}{\partial S_a}\right)^k\nabla S_a^{k+1}$$
$$+\left(\frac{\partial S_v}{\partial \rho_\ell}\right)^k\nabla\rho_\ell^{k+1} + \left(\frac{\partial S_v}{\partial \rho_v}\right)^k\nabla\rho_v^{k+1} + \left(\frac{\partial S_v}{\partial \rho_a}\right)^k\nabla\rho_a^{k+1},$$

and the upwind operator $\{\cdot\}^{\uparrow}$ defined in the following section.

4.6 | Upwind scheme

To facilitate the transport of phases by the total Darcy velocity $\mathbf{u}_t$, an upwind scheme is used to approximate fluxes across interfaces for the term $\left(F_g^k + \left(\frac{\partial F_g}{\partial z_g}\right)^k(z_g^{k+1}-z_g^k)\right)\mathbf{u}_t^{*,k+1}\cdot\mathbf{n}_e$. Let us fix an interior face e that is shared by two mesh elements K_i and K_o such that $\mathbf{n}_e$ is outward of K_i. For readibility, we denote the fluxes as follows

$$D = F_g^k + \left(\frac{\partial F_g}{\partial z_g}\right)^k(z_g^{k+1}-z_g^k), \qquad D^{\mathrm{grav}} = x_{g,\ell}\rho_\ell^2\lambda_\ell + x_{g,v}\rho_v^2\lambda_v.$$

The upwind value $\left\{\left(F_g^k + \left(\frac{\partial F_g}{\partial z_g}\right)^k(z_g^{k+1}-z_g^k)\right)\mathbf{u}_t^{*,k+1}\cdot\mathbf{n}_e\right\}^{\uparrow}$ across the face e is then computed as follows:

$$\left\{\left(F_g^k + \left(\frac{\partial F_g}{\partial z_g}\right)^k(z_g^{k+1}-z_g^k)\right)\mathbf{u}_t^{*,k+1}\cdot\mathbf{n}_e\right\}^{\uparrow} = \begin{cases}\frac{1}{2}D\big|_{K_i}((\mathbf{u}_t^{*,k+1})|_{K_i} + (\mathbf{u}_t^{*,k+1})|_{K_o})\cdot\mathbf{n}_e & \text{if } \xi\geq 0,\\ \frac{1}{2}D\big|_{K_o}((\mathbf{u}_t^{*,k+1})|_{K_i} + (\mathbf{u}_t^{*,k+1})|_{K_o})\cdot\mathbf{n}_e & \text{if } \xi < 0.\end{cases}$$

where

$$\xi = ((D\mathbf{u}_t + D^{\mathrm{grav}}\mathbf{g})|_{K_i} + (D\mathbf{u}_t + D^{\mathrm{grav}}\mathbf{g})|_{K_o})\cdot\mathbf{n}_e \tag{4.19}$$

5 | STUDY OF ALGORITHM'S CONVERGENCE PROPERTIES

In this section we use manufactured solutions to test the convergence properties of our scheme, that we have implemented within the DUNE framework [32–35] We introduce a set of solutions of a three-phase black oil problem on a two dimensional domain. Two sets of fluids properties are considered. The first case uses fluids with the same densities and viscosities. It allows us to show the benefits of using the subiteration scheme introduced in Section 3.3. The second test shows the correct behavior of the algorithm with phases of different densities and viscosities. The parameters, such as the time and density, involved in the numerical tests are all expressed in International System of Units (SI).

5.1 | Manufactured solutions and test set up

The following tests aim to approximate the set of manufactured solutions defined as follows:

$$p_\ell(t,x,y) = (2 + xy^2 + x^2\sin(t+y)), \tag{5.1}$$

$$S_\ell(t,x,y) = \frac{2 - x^2y^2}{4}, \tag{5.2}$$

$$S_v(t,x,y) = \frac{3 - \cos(t+x)}{8}, \tag{5.3}$$

$$S_a(t,x,y) = \frac{1 + 2x^2y^2 + \cos(t+x)}{8}, \tag{5.4}$$

where the variable z_g can be shown to be equal to:

$$z_g(t,x,y) = \frac{3 - \cos(t+x)}{8}. \tag{5.5}$$

The computational domain is the unit square $\Omega = [0,\,1]^2$. The porosity of the domain is constant equal to 0.2 everywhere. The phase relative permeabilities, respectively the capillary pressures, are defined as follows [36, 37]:

$$\kappa_{abs} = 1, \qquad \kappa_\ell = S_\ell(S_\ell + S_a)(1 - S_a), \qquad \kappa_v = S_v^2, \qquad \kappa_a = S_a^2. \tag{5.6}$$

$$p_{c,v} = \frac{3.9}{\ln(0.01)}\ln(1 - S_v + 0.01), \qquad p_{c,a} = \frac{6.3}{\ln(0.01)}\ln(S_a + 0.01). \tag{5.7}$$

We note that for this example, mass transfers are not considered so we set:

$$x_{g,\ell} = 0, \qquad x_{o,\ell} = 1, \qquad x_{g,v} = 1, \qquad x_{o,v} = 0. \tag{5.8}$$

Once the phases densities and viscosities are set, the term sources q_l, q_v and q_a are computed accordingly. The convergence tests are performed on a set of six uniform grids with respective mesh size $h \in \{0.2,\, 0.1,\, 0.05,\, 0.025,\, 0.0125,\, 0.00625\}$. The convergence properties are evaluated by using a time step τ that is set proportional to h or h^2 with a final time $T = 1$. As our scheme is first order in time and space, we expect the convergence rate in the L^2 norm to be of order one when $\tau = h$ and order two with $\tau = h^2$.

5.2 | Tests with three components of equal densities and viscosities

We consider a fluid composed of phases that share the same densities and the same viscosities, all set equal to one. We compare in Table 1 the results obtained with our algorithm when the subiteration

TABLE 1 Convergence tests with components of equal densities and viscosities. The mesh size is denoted by h and the number of degrees of freedom per unknown by n_{df}. The time step τ is set to the mesh size h. Tolerance of subiteration scheme set to 10^{-7} when used

L^2-norm of error		Liquid pressure		Aqueous saturation		Gas fraction z_g	
h	n_{df}	Error	Rate	Error	Rate	Error	Rate
No subiteration							
0.2	25	3.16E−03	–	3.01E−02	–	4.86E−02	–
0.1	100	9.69E−04	1.71	8.30E−03	1.86	1.45E−02	1.74
0.05	400	5.10E−04	0.93	6.13E−03	0.44	4.02E−03	1.85
0.025	1,600	3.04E−04	0.75	4.16E−03	0.56	1.31E−03	1.62
0.0125	6,400	1.74E−04	0.80	2.43E−03	0.78	7.33E−04	0.84
With subiteration							
0.2	25	2.68E−03	–	4.23E−02	–	4.35E−02	–
0.1	100	5.11E−04	2.39	1.24E−02	1.77	1.41E−02	1.63
0.05	400	1.20E−04	2.09	3.72E−03	1.74	4.02E−03	1.81
0.025	1,600	4.13E−05	1.54	1.12E−03	1.73	9.48E−04	2.08
0.0125	6,400	2.75E−05	0.59	3.47E−04	1.69	2.40E−04	1.98

scheme, introduced in Section 3.3, is either disabled or enabled with a tolerance set to 10^{-7}. These computations were done with a time step τ set to the mesh size h. The relative errors displayed when the subiteration scheme is disabled are consistent with an algorithm of order one. When the subiteration scheme is used, the rate of convergence is often close to two and the relative errors associated to the three unknowns p_ℓ, S_a and z_g are better than the relative errors obtained without subiteration.

We conclude that it is preferable to use the subiteration scheme when the time step follows a Courant–Friedrichs–Lewy (CFL) like condition where τ is proportional to h. More information on CFL can be found in [38].

5.3 | Tests with three components of different densities and viscosities

We consider the same solutions and settings introduced previously except that we set the densities and viscosities as follows:

$$\rho_l = 3, \qquad \rho_v = 1, \qquad \rho_a = 5, \tag{5.9}$$

$$\mu_l = 0.75, \qquad \mu_v = 0.25, \qquad \mu_a = 0.5. \tag{5.10}$$

Due to the approximation of the time derivative in the z_g equation, the problem is approximated with the subiteration scheme. Indeed at the first subiteration, the term $\frac{\phi^{k+1}\rho_t^{k+1}z_g^{k+1}}{\tau}$ uses the saturation at time t_n to approximate the quantity ρ_t^{k+1}. As the term ρ_t depends of the time, an error of order zero is introduced in the first subiteration. It drives us to approximate this problem with the subiteration scheme where the tolerance is set to 10^{-7}. The results are displayed in Table 2. In this case, the relative errors using a time step τ set to $h/10$ are very similar to the one where $\tau = h^2/10$ (up to 10–20%). It indicates that the error is dominanted by an error in space. The rate of convergence tends to two in both case which is consistant with the use of finite element of order one.

The results presented in this section show that our algorithm behaves as expected for three-phase black oil problem involving variable fluid properties and capillary pressure effects. As mentioned in Sections 5.2, the subiteration scheme greatly improves the approximations for time step of same order

TABLE 2 Convergence tests with components of different densities and viscosities. Subiteration's tolerance set to 10^{-7}. The mesh size is denoted by h the time step by τ and the degrees of freedom per unknown by n_{df}

L^2-norm of error		Liquid pressure		Aqueous saturation		Gas fraction z_g	
h	n_{df}	Error	Rate	Error	Rate	Error	Rate
$\tau = h/10$							
0.2	25	2.58E−03	–	4.53E−02	–	9.20E−02	–
0.1	100	1.02E−03	1.34	1.34E−02	1.76	3.02E−02	1.61
0.05	400	3.80E−04	1.42	3.99E−03	1.75	9.57E−03	1.66
0.025	1,600	1.20E−04	1.66	1.14E−03	1.81	2.83E−03	1.76
0.0125	6,400	3.16E−05	1.93	3.06E−04	1.90	7.64E−04	1.89
$\tau = h^2/10$							
0.2	25	2.67E−03	–	4.56E−02	–	9.34E−02	–
0.1	100	1.11E−03	1.27	1.36E−02	1.75	3.10E−02	1.59
0.05	400	4.29E−04	1.37	4.09E−03	1.73	9.98E−03	1.64
0.025	1,600	1.46E−04	1.56	1.19E−03	1.78	3.04E−03	1.71

than the mesh size. As a consequence, all the computations reported in the rest of the paper use the subiteration scheme with a tolerance set to 10^{-3}.

6 | ACTION OF GRAVITY ON A WATER INJECTION PROBLEM

We study the effect of gravity in a two component-two phase injection problem, with no mass transfer between the phases. The porous medium is a vertical rectangular column filled with oil in liquid phase. The aqueous phase (water) is injected from the top horizontal face of the medium. As expected, our results show that the presence of gravity can either increase or slow the front propagation of the wetting phase, depending of its orientation in the vertical direction.

6.1 | Problem setting

We consider a three-dimensional domain $\Omega = [0, 10] \times [0, 10] \times [0, 100]$. The system is composed of a liquid phase and an aqueous phase with the following properties:

$$\phi = 0.2, \qquad \rho_\ell = 800, \qquad \rho_a = 1000, \qquad \mu_\ell = 10^{-3}, \qquad \mu_a = 8.9 \times 10^{-4}, \tag{6.1}$$

$$\kappa_\ell = S_\ell^2, \qquad \kappa_a = S_a^2, \qquad \kappa_{\text{abs}} = 6.24 \times 10^{-13}. \tag{6.2}$$

The capillary pressure is based on the Brooks-Corey [39] model.

$$p_{c,a} = \begin{cases} S_a^{-0.5} \times 10^5 & \text{if } S_a > 0.05, \\ (1.5 - 10 S_a) \times 0.05^{-0.5} \times 10^5 & \text{otherwise.} \end{cases} \tag{6.3}$$

Initially, the medium is mainly filled with oil with an initial liquid saturation $S_\ell|_{(t=0)} = 0.9$. Water is injected from the top horizontal face via the following Dirichlet boundary condition:

$$S_a|_{z=100} = 0.1 + 0.67 \frac{(t/10^5)^3}{1 + (t/10^5)^3}. \tag{6.4}$$

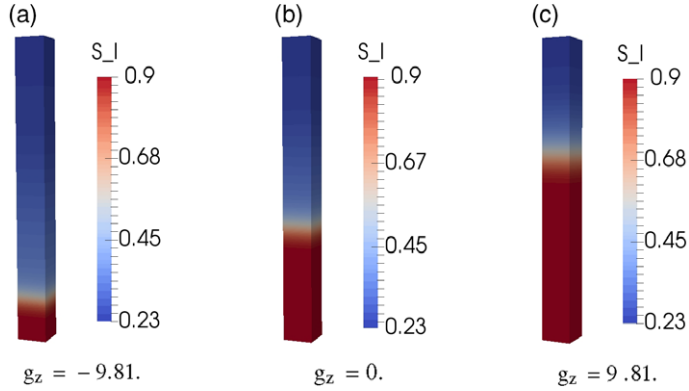

FIGURE 1 Snapshots of the liquid saturation profile for various gravities at the time $T = 10^6$. $\Omega = [0, 10] \times [0, 10] \times [0, 100]$ with $h = 1$ [Color figure can be viewed at wileyonlinelibrary.com]

To let the water fills the container, the pressure is set to a linear profile in the vertical direction as follows:

$$p_\ell|_{t=0} = 2 \times 10^6 - 2(100 - z) \times 10^4 \tag{6.5}$$

This initial condition is used as a Dirichlet pressure boundary condition on the faces ($z = 0$) and ($z = 100$). Homogeneous Neumann conditions are applied elsewhere. Mass transfer effect or source terms are not considered such that the rate of injection of water mainly depends of the pressure profile and the gravity that is set to:

$$\mathbf{g} = (0, 0, g_z)^T. \tag{6.6}$$

where g_z is a real to set. The propagation speed of the water then depends of the quantity $\nabla p_\ell - \rho_a \mathbf{g}$ involved in the transport terms of Equation (3.3). We note that capillarity effect also plays a role in the transport of the water.

6.2 | Influence of gravity on front propagation

We study three cases where the vertical component g_z of the gravity $\mathbf{g}$ is set to either -9.81, 0 and 9.81. The case $g_z = 0$ correspond to an injection problem without gravity effect while the case $g_z = 9.81$ can be seen as a test with gravity effect modulo a change of frame for the vertical direction. The computations presented in this section use a uniform grid with a mesh size $h = 1$ and a time step set to $\tau = 10^4$ (CFL ~ 0.14).

Figure 1 shows 3D snapshots of the liquid saturation for the three different cases at time $T = 10^6$. As the pressure gradient is negative in the vertical direction, we recover that the front propagation is accelerated for $g_z = -9.81$, respectively reduced for $g = 9.81$, with respect to the computation without gravity effect.

The time evolution of the aqueous saturation at the point (5, 5, 50) is displayed in Figure 2. The saturation S_a reaches a level of 0.7 at the time $T = 9 \times 10^5$ for $g = -9.81$, respectively $T = 1.2 \times 10^6$ for $g = 0$ and $T = 1.9 \times 10^6$ for $g = 9.81$. It shows that the water is propagating 1.33 times faster with $g = -9.81$, respectively 1.58 times slower with $g = 9.81$, than with $g = 0$. As the magnitude of the vertical component of the pressure gradient is roughly equal to two times $\rho_a \times 9.81$, disregarding the effect of the capillary pressure would lead us to expect the injected water to fill the container 1.5 times faster with $g = -9.81$, respectively two times slower with $g = 9.81$, compared to the case without gravity. The results obtained by our algorithm are coherent with this prediction.

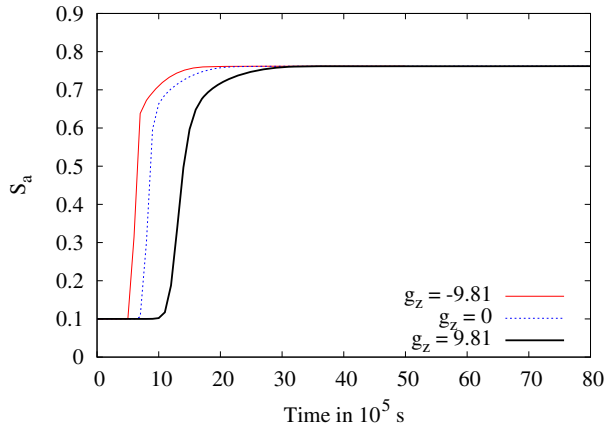

FIGURE 2 Time evolution of the liquid saturation for various gravities at the point (5, 5, 50) [Color figure can be viewed at wileyonlinelibrary.com]

7 | MASS TRANSFER WITHIN A THREE-COMPONENT THREE-PHASE SYSTEM

We test our numerical scheme with a flow problem involving mass transfer between the liquid and vapor phases in a three-dimensional heterogeneous medium. Both gas and water are injected in a porous medium initially saturated with oil in liquid phase. Depending of the local pressure, the gas component can be found in liquid and/or vapor phase. The oil component is forced to remain in liquid phase by setting $x_{g,v} = 1$.

7.1 | A mechanism of mass transfer

The set up considered in this section relies on the idea that gas tends to be in vapor phase under low pressure and in liquid phase under high pressure. To study a problem involving mass transfer, we introduce two threshold pressures $p^0_{\text{thr}} = 2 \times 10^8$ and $p^1_{\text{thr}} = 3 \times 10^8$ such that the gas component is entirely in vapor phase for pressures lower than p^0_{thr} and entirely in liquid phase for pressures higher than p^1_{thr}.

Following [30], the oil and gas mass fractions in the liquid phase depend on the liquid phase pressure:

$$x_{o,\ell} = \frac{\rho_\ell^{\text{STD}}}{\rho_\ell^{\text{STD}} + \rho_v^{\text{STD}} f(p_\ell)}, \qquad x_{g,\ell} = \frac{\rho_v^{\text{STD}} f(p_\ell)}{\rho_\ell^{\text{STD}} + \rho_v^{\text{STD}} f(p_\ell)}, \tag{7.1}$$

where $\rho_\ell^{\text{STD}} = 100$ and $\rho_v^{\text{STD}} = 800$ are the liquid and vapor densities at standard conditions. Unlike [30] where the volumetric gas fraction dissolved in the liquid phase f is defined as in [40], we consider a function f that is an increasing function of p_ℓ made to be constant for pressures lower than p^0_{thr} and higher than p^1_{thr}. The function f is defined as follows:

$$f(p_\ell) = \begin{cases} 0 & \text{if } p_\ell < p^0_{\text{thr}} \\ 0.4\left(1.0 + \frac{p^*((p^*)^2 - 3.0\epsilon^2)}{-2.0\epsilon^3}\right) & \text{if } p^0_{\text{thr}} < p_\ell < p^1_{\text{thr}} \\ 0.8 & \text{otherwise.} \end{cases} \tag{7.2}$$

where $p^* = \frac{p_\ell - 0.5(p^1_{\text{thr}} + p^0_{\text{thr}})}{2}$ and $\epsilon = \frac{p^1_{\text{thr}} - p^0_{\text{thr}}}{2}$. Figure 3 displays the profile $x_{g,\ell}$.

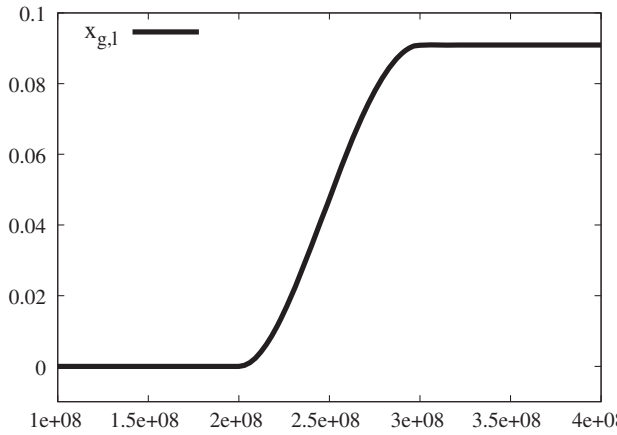

FIGURE 3 Profile of the gas mass fraction $x_{g,\ell}$ as a function of liquid phase pressure

7.2 | Phases properties. Problem's initial and boundary conditions

The domain of computation Ω is set to $[0, 1{,}000] \times [0, 100] \times [0, 100]$. The densities and viscosities of the liquid, vapor and aqueous phases are:

$$\mu_a = \mu_\ell = 10^{-3}, \quad \mu_v = 10^{-4}, \quad \rho_\ell = \frac{\rho_\ell^{\mathrm{STD}} + \rho_v^{\mathrm{STD}} f(p_\ell)}{B_o}, \quad \rho_v = \frac{\rho_v^{\mathrm{STD}}}{B_g}, \quad \rho_a = 1000. \tag{7.3}$$

where f is defined by (7.2), B_g and B_o are the gas and oil formation volume factors introduced in [40]. We set $B_g = 0.25$ and $B_o = 1$. The porosity and relative permeabilities are:

$$\phi = 0.2, \qquad \kappa_\ell = S_\ell^2, \qquad \kappa_v = S_v^2, \qquad \kappa_a = S_a^2. \tag{7.4}$$

The porous medium is heterogeneous as the absolute permeability of the media is discontinuous.

$$\kappa_{\mathrm{abs}} = \begin{cases} 6.24 \times 10^{-13} & \text{if } (x, y, z) \in [100, 200] \times [30, 70] \times [0, 100] \\ 6.24 \times 10^{-12} & \text{otherwise.} \end{cases} \tag{7.5}$$

The capillary pressure are defined with a formula based on the one of Brooks-Corey [39] with $\lambda = 2$. It reads:

$$p_{c,v} = \begin{cases} -S_v^{-0.5} \times A_{pc} & \text{if } S_v > 0.05, \\ (-1.5 + 10 S_v) \times 0.05^{-0.5} \times A_{pc} & \text{otherwise,} \end{cases} \tag{7.6}$$

and

$$p_{c,a} = \begin{cases} S_a^{-0.5} \times A_{pc} & \text{if } S_a > 0.05, \\ (1.5 - 10 S_a) \times 0.05^{-0.5} \times A_{pc} & \text{otherwise,} \end{cases} \tag{7.7}$$

where A_{pc} is set to 10^7.

The reservoir is initially saturated with liquid, meaning $(S_\ell, S_v, S_a)|_{t=0} = (1, 0, 0)$, and the initial pressure is set to:

$$p_\ell|_{t=0} = 4.0 \times 10^8 - 10^5 x. \tag{7.8}$$

We note that under these conditions, the initial liquid phase is composed of roughly 9% of gas and 91% of oil. Water is injected by enforcing the following Dirichlet boundary conditions on the

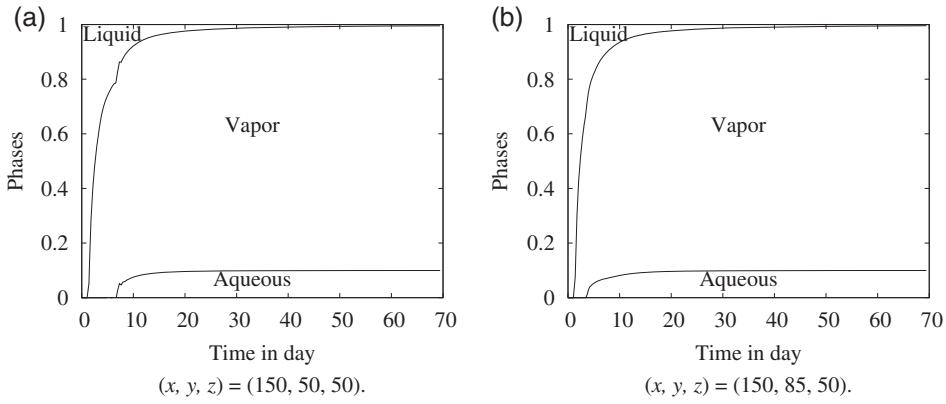

FIGURE 4 Time evolution of the phases distribution at different locations (x, y, z). The quantity S_a is represented by the lower line and the quantity $S_v + S_a$ is represented by the upper line

variable S_a:

$$S_a|_{(x=0)} = \frac{\bar{t}^3}{10(1+\bar{t}^3)}, \tag{7.9}$$

with $\bar{t} = t \times 10^{-5}$ where the time is denoted by t. The liquid phase pressure in the reservoir is then slowly reduced by setting:

$$p_\ell|_{(x=0)\cup(x=10^3)} = 4.0 \times 10^8 - 10^5 x - 2.0 \times 10^8 \frac{\bar{t}^3}{1+\bar{t}^3}. \tag{7.10}$$

It allows us to inject a fluid composed of gas or a mixture gas–oil depending of the pressure magnitude. It is done by imposing the following conditions on the saturation S_ℓ:

$$S_\ell|_{x=0} = \begin{cases} 1 - S_a|_{x=0} & \text{if } p_\ell > 3 \times 10^8, \\ 1 - S_a|_{x=0} - (2.7 - 9p_\ell|_{x=0} \times 10^{-9}) & \text{if } 2 \times 10^8 < p_\ell|_{x=0} < 3 \times 10^8, \\ 0 & \text{otherwise.} \end{cases} \tag{7.11}$$

We note that S_a tends to 0.1 as p_ℓ gets closer to 2×10^8 which makes the above boundary condition continuous in time. The corresponding Dirichlet condition on the variable z_g can be deduced from Equations (2.3) and (3.2). Homogeneous Neumann conditions are applied to p_ℓ,S_a and z_g elsewhere.

7.3 | Numerical results

We study the above setting with a uniform grid of mesh size $h = 10$ and a time step $\tau = 10^3$ s, meaning 0.012 day (CFL ~ 0.624). As the computational time grows, we expect the liquid phase to disappear for the benefit of a vapor-aqueous system composed of gas and water with $S_v = 0.9$ and $S_a = 0.1$. Indeed, for large time the pressure magnitude becomes smaller than 2×10^8. As a consequence the fluids injected are gas and water with respective saturation $S_v = 0.9$ and $S_a = 0.1$. Figure 4 displays the time evolution of the phase distribution at the locations (50, 50, 50) and (85, 50, 50). We recover the expected behavior as the liquid phase disappears with time while the aqueous saturation grows to 10% (see lower black lines). Moreover, the plot shows that the vapor and aqueous phases are propagating faster in the region of higher mobility. We also note that the evolution of the phase distributions is smoother with time as no discontinuity of the media's permeability is encountered.

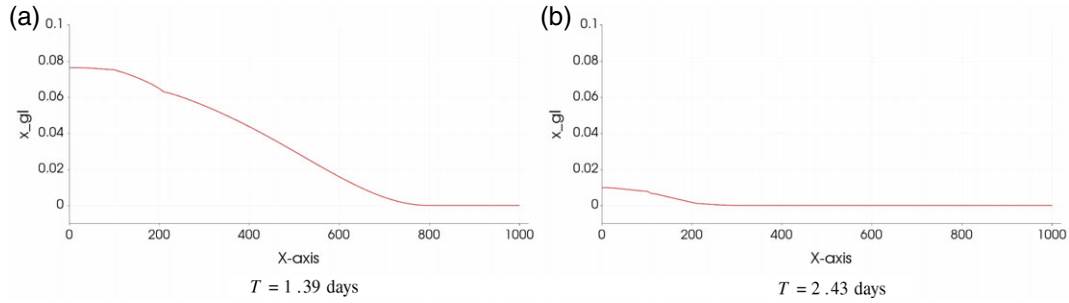

FIGURE 5 Profile of the mass fraction x_{gl} along the line $(y = 50) \cap (z = 50)$ at different times T [Color figure can be viewed at wileyonlinelibrary.com]

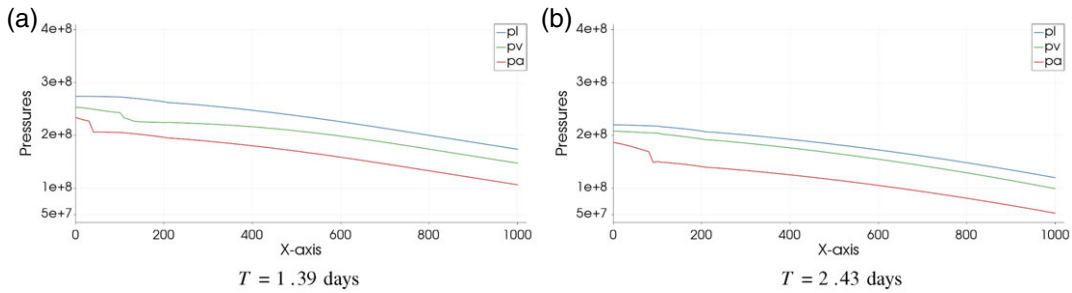

FIGURE 6 Profile of the pressures along the line $(y = 50) \cap (z = 50)$ at different times T. (a) p_ℓ in blue, (b) p_v in green, (c) p_a in red [Color figure can be viewed at wileyonlinelibrary.com]

During the early transient regime, meaning $t \leq 2 \times 10^5\, s$ (i.e., 2.3 days) such that $\frac{\bar{t}^3}{1+\bar{t}^3} \leq 0.9$, the system is mainly composed of liquid and vapor phases. While the vapor phase is exclusively composed of gas, due to imposing $x_{g,\ell} = 1$, Figure 5 shows that the liquid phase is a mixture of oil and gas. As time increases, the fraction of gas in the liquid phase tends to zero. This component disappearance happens first in area close to the region $x = 10^3$. It is consistent with the boundary conditions imposed to the liquid pressure as $p_\ell|_{x=1{,}000}$ goes under 2×10^8 before $p_\ell|_{x=0}$. Figure 6 displays the profile of the pressures on the same line and at the same times used to represent $x_{g,\ell}$ in Figure 5. It shows that the liquid pressure becomes smaller than 2×10^8 for $x \geq 800$ at time $T = 1.39$ days and at time $T = 2.43$ days for $x \geq 200$. These results are consistent with the profile of $x_{g,\ell}$ where this mass fraction is zero for $x \geq 200$ at time $T = 2.43$ days and for $x \geq 800$ at time $T = 1.39$ days.

In Figure 7, we display snapshots of the liquid saturation to show the influence of the low mobility region in the transport of the injected components. We recall that the low mobility area is represented by the region $[100, 200] \times [30, 70] \times [0, 100]$. It has an absolute permeability 10 times smaller than in the rest of the reservoir. Figure 7a shows that the injected phases are not flooding the low permeability region as the liquid phase remains high there. As the time incrases, the injected phases manage to recover a homogeneous vertical front of propagation as shown in Figure 7b near the plan $(x = 300)$.

8 | RANDOM DISTRIBUTION OF ABSOLUTE PERMEABILITY

We investigate the robustness of our algorithm for problem involving highly heterogeneous media. The three-phase three-component set up consists of injecting a mixture of gas and water in a reservoir

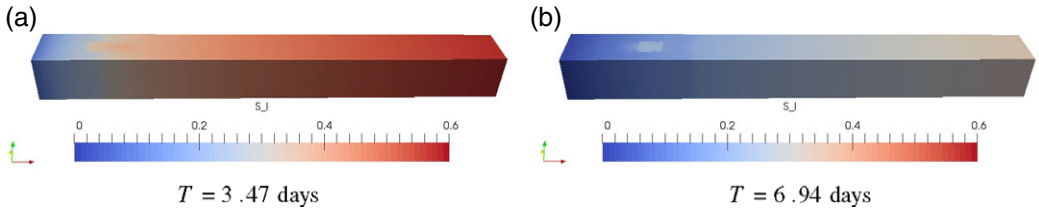

FIGURE 7 Snapshots of the liquid saturation profile at various times T [Color figure can be viewed at wileyonlinelibrary.com]

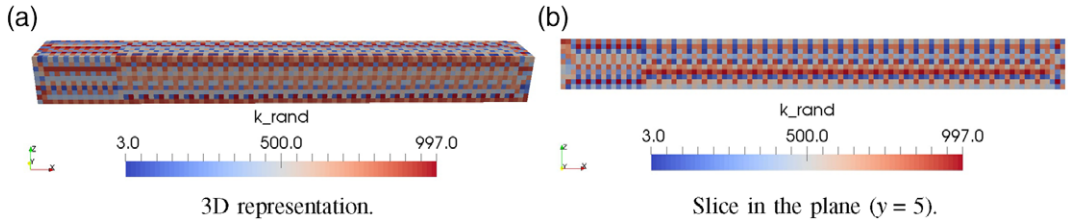

FIGURE 8 Distribution of the random permeability κ_{rand}. The effective permeability is multiplied by $\kappa_{\text{ref}} = 6.24 \times 10^{-13}$ [Color figure can be viewed at wileyonlinelibrary.com]

mainly filled with oil. The absolute permeability is made highly heterogeneous by generating it randomly on each grid cell with a ratio of magnitude of order 10^3. The dimension of the reservoir, denoted by Ω, is set to $[0, 100] \times [0, 10] \times [0, 10]$.

8.1 | Injection with an absolute permeability generated randomly

The three phase fluids system considered has the same physical properties than the test of Section 7 up to one exception: we set $f = 0$. We recall that f was previously defined in Equation (7.2). Setting this function to zero means that $x_{g,\ell} = 0$ such that mass transfer does not occur. We refer to Equations (7.3) and (7.4) for a definition of the porosity and the fluids densities, viscosities and permeabilities. The absolute permeability of the reservoir is defined as follows:

$$\kappa_{\text{abs}}(x, y, z) = \kappa_{\text{rand}} \kappa_{\text{ref}} \tag{8.1}$$

where κ_{ref} is set to 6.24×10^{-13}. The function κ_{rand} is a piecewise constant function that takes value in $[1, 10^3]$. Its values on the grid's cells are generated randomly. Figure 8 displays the three-dimensional distribution of κ_{rand} in the domain Ω. A two dimensional representation, in the plane $(y = 5)$, is also shown. It confirms that the absolute permeability considered in this test is highly heterogeneous in the whole domain. The capillary pressures are defined as in Section 7 where the coefficient A_{pc} is set to 10^6.

The reservoir is initially filled with a mixture of liquid and vapor phases by setting:

$$(S_\ell, S_v, S_a)|_{t=0} = (0.9, 0.1, 0). \tag{8.2}$$

The initial pressure is defined as follows:

$$p_\ell|_{t=0} = 2.0 \times 10^7 - x \times 10^5. \tag{8.3}$$

Dirichlet boundary conditions that matches the liquid pressure initial condition are applied on the faces $(x = 0)$ and $(x = 100)$. The following boundary conditions are enforced on the aqueous and vapor

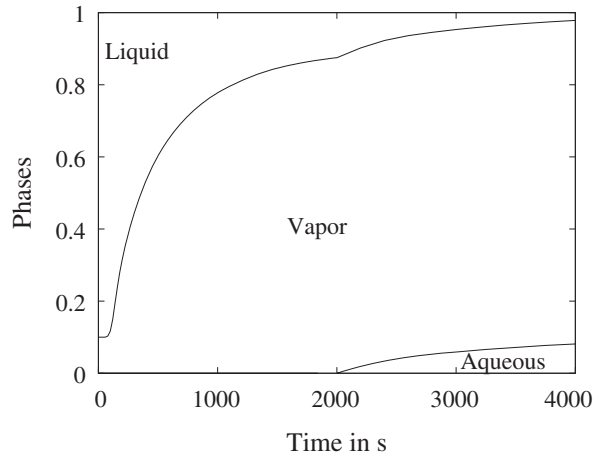

FIGURE 9 Time evolution of the phases distribution at the point (40, 5, 5). The quantity S_a is represented by the lower line and the quantity $S_v + S_a$ is represented by the upper line. $\Omega = [0, 100] \times [0, 10] \times [0, 10]$ with $h = 1$

saturations:

$$S_a|_{(x=0)} = \frac{\bar{t}^3}{10(1+\bar{t}^3)}, \qquad S_v|_{(x=0)} = 0.1 + \frac{8\bar{t}^3}{10(1+\bar{t}^3)} \tag{8.4}$$

with $\bar{t} = t \times 10^{-2}$. The Dirichlet conditions imposed to the variable z_g can be derived from Equations (2.3) and (3.2). Homogeneous Neumann conditions are applied to p_ℓ, S_a and z_g elsewhere.

The set up is approximated with a uniform grid of mesh size $h = 1$. The time step τ is set to 0.5 (CFL ~ 0.312). Figure 9 displays the time evolution of the phase distribution at the point (40, 5, 5). The propagation of gas in the reservoir is represented by a smooth curve till water appears around the time $T = 2{,}000$ s. At this instant, the vapor saturation has nearly reached its asymptotic value equal to 0.9. Thus, for time $T \geq 2{,}000$ s the remaining liquid phase is replaced with water. This figure alone could lead us to believe that the front propagation of gas and water in the media is acting similarly than in a case with homogeneous media. However this local behavior does not reflect how the gas and water propagate in the reservoir. To have a better understanding, we show in Figure 10 a threshold of the three-dimensional profile of the aqueous saturation at different times. The minimum value of the threshold is set to 0.01 and the maximum value to 0.1. We can notice the appearance of fingering effect, phenomena that is known to occur in highly heterogeneous media see [15, 41–45]. Indeed, the front of propagation of the water component is not anymore a flat vertical surface and so even after a large computational time. Due to the presence of high and low mobility regions, located randomly in the reservoir, the injected water follows the direction that are more optimal to its propagation which lead to the creation of little fingers. Similar behavior can be observed with the oil component.

8.2 | Random permeability with a channel of higher magnitude

We consider the same set up and numerical resolution than previously apart that the absolute permeability is generated as follows:

$$\kappa_{\text{abs}}(x, y, z) = \begin{cases} \kappa^1_{\text{rand}} \kappa_{\text{ref}} & \text{if } 3 \leq z \leq 7, \\ \kappa^2_{\text{rand}} \kappa_{\text{ref}} & \text{otherwise,} \end{cases} \tag{8.5}$$

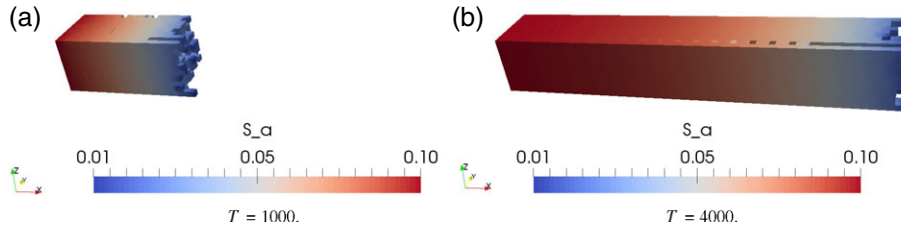

FIGURE 10 Threshold of the aqueous saturations in a 3D rendering. Minimum value represented is $S_a = 0.01$ and maximum value represented is $S_a = 0.1$ [Color figure can be viewed at wileyonlinelibrary.com]

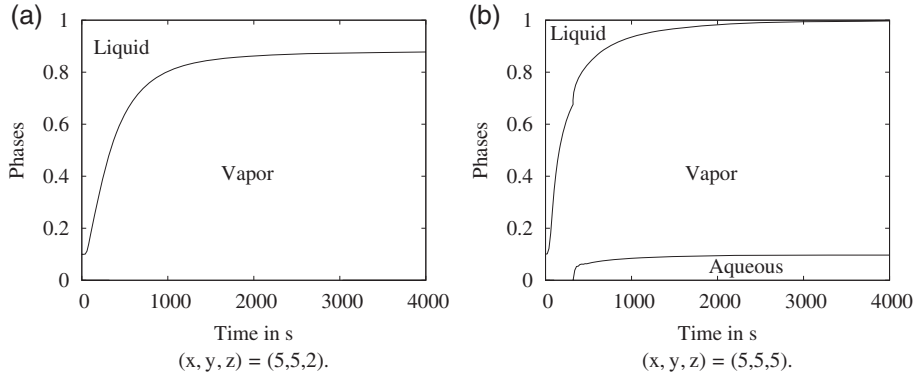

FIGURE 11 Time evolution of the phases distribution at different points (x, y, z). (a) The quantity S_v is represented by the black line. (b) the quantity S_a is represented by the lower line and the quantity $S_v + S_a$ is represented by the upper line. $\Omega = [0, 1{,}000] \times [0, 100] \times [0, 100]$ with $h = 10$

where κ_{ref} is set to 6.24×10^{-13}. The functions κ^1_{rand} and κ^2_{rand} are piecewise constant functions that takes value in [50, 1,050], respectively [1, 10]. This permeability is considered to create a region of high mobility represented by the channel $[0, 100] \times [0, 10] \times [3, 7]$. Figure 11 displays the time evolution of the phases distribution at the points (5, 5, 2) and (5, 5, 5). The vapor and aqueous phases are propagating faster at the point (5, 5, 5) as it is inside the channel of higher mobility. Indeed, the aqueous phase start to appear around the time 400 s at the point (5, 5, 5) while it does not appear after 4,000 s at the point (5, 5, 2). This difference is consistent with the difference of absolute permeability that is in average 100 times larger in the channel than in the rest of the media.

Fingering effect similar to the one observed in the previous Section 8.1 can be observed as shown in Figure 12. This figure displays the region where the aqueous saturation is in the interval [0.01, 0.1] at the time 2,000 and 4,000 s. Small fingering effects can be seen near the two fronts of propagation, one in the high mobility region and one near the face $x = 0$ outside the channel. Such effects could be more accentuated by adding gravity effects or setting different order of magnitude for the aqueous and liquid viscosity.

9 | CONCLUSION AND PERSPECTIVES

We have introduced a new time and space discretization technique that uses a DG method to approximate the three-phase and three-component black oil problem. The algorithm is based on the formulations introduced in [12, 30]. The scheme allows for the occurrence of mass transfer between the

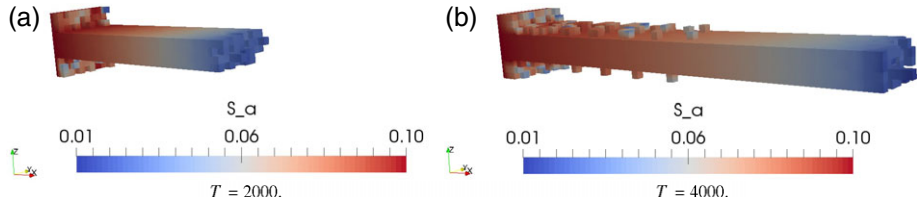

FIGURE 12 Threshold of the aqueous saturations in a 3D rendering. Minimum value represented is $S_a = 0.01$ and maximum value represented is $S_a = 0.1$ [Color figure can be viewed at wileyonlinelibrary.com]

liquid and vapor phases. It has been validated on numerous problems ranging from convergence tests with manufactured solutions to more physical set up that involve gravity and phase disappearance. The robustness of the algorithm has been checked on highly heterogeneous media where the absolute permeability varies over three-order of magnitude. The benefits of using high order finite element is currently being investigated for viscous fingering problem. Future studies are also engaged to show the ability of our algorithm to approximate well production problem [47]. Qualitative and performance comparisons between this technique and codes using different formulation or approximation method on benchmarks [46] are being considered.

ORCID

Loïc Cappanera https://orcid.org/0000-0002-3871-1073

REFERENCES

[1] K. Aziz, A. Settari, *Petroleum reservoir simulation*, Applied Science Publ. Ltd., London, UK, 1979.
[2] Z. Chen, G. Huan, Y. Ma, *Computational methods for multiphase flows in porous media*, vol. 2, SIAM, Philadephia, Pennsylvania, USA, 2006.
[3] D. W. Peaceman, *Fundamentals of numerical reservoir simulation*, vol. 6, Elsevier, Amsterdam, Netherlands, 2000.
[4] G. Acs, S. Doleschall, E. Farkas, *General purpose compositional model*, Soc. Petrol. Eng. J. vol. 25 (1985) pp. 543–553.
[5] Z. Chen, *Formulations and numerical methods of the black oil model in porous media*, SIAM J. Numer. Anal. vol. 38(2) (2000) pp. 489–514.
[6] K. H. Coats, *An equation of state compositional model*, Soc. Petrol. Eng. J. vol. 20(05) (1980) pp. 363–376.
[7] L. Fussell, D. Fussell, et al., *An iterative technique for compositional reservoir models*, Soc. Petrol. Eng. J. vol. 19(04) (1979) pp. 211–220.
[8] L. Nghiem, "*A new approach to quasi-newton methods with application to compositional modeling*," in *SPE Reservoir Simulation Symposium*, Society of Petroleum Engineers, Richardson, Texas, USA, 1983, pp. 83–91 SPE 12242.
[9] J. A. Trangenstein, J. B. Bell, *Mathematical structure of the black-oil model for petroleum reservoir simulation*, SIAM J. Appl. Math. vol. 49(3) (1989) pp. 749–783.
[10] J. Watts, *A compositional formulation of the pressure and saturation equations*, SPE Reserv. Eng. vol. 1(03) (1986) pp. 243–252.
[11] L. C. Young, R. E. Stephenson, *A generalized compositional approach for reservoir simulation*, Soc. Pet. Eng. J. vol. 23(05) (1983) pp. 727–742.
[12] G. Shank, C. Vestal, et al., *Practical techniques in two-pseudocomponent black-oil simulation*, SPE Reserv. Eng. vol. 4(02) (1989) pp. 244–252.
[13] A. Ern, A. F. Stephansen, P. Zunino, *A discontinuous galerkin method with weighted averages for advection–diffusion equations with locally small and anisotropic diffusivity*, IMA J. Numer. Anal. vol. 29(2) (2008) pp. 235–256.
[14] A. Ern, S. Nicaise, M. Vohralík, *An accurate h (div) flux reconstruction for discontinuous galerkin approximations of elliptic problems*, Comptes Rendus Mathematique vol. 345(12) (2007) pp. 709–712.
[15] J. Li, B. Riviere, *High order discontinuous galerkin method for simulating miscible flooding in porous media*, Comput. Geosci. vol. 19(6) (2015) pp. 1251–1268.

[16] T. Arbogast et al., *A discontinuous galerkin method for two-phase flow in a porous medium enforcing* h *(div) velocityand continuous capillary pressure*, Comput. Geosci. vol. 17(6) (2013) pp. 1055–1078.
[17] P. Bastian, *A fully-coupled discontinuous galerkin method for two-phase flow in porous media with discontinuous capillary pressure*, Comput. Geosci. vol. 18(5) (2014) pp. 779–796.
[18] Y. Epshteyn, B. Riviere, *Fully implicit discontinuous finite element methods for two-phase flow*, Appl. Numer. Math. vol. 57 (2007) pp. 383–401.
[19] A. Ern, I. Mozolevski, L. Schuh, *Discontinuous galerkin approximation of two-phase flows in heterogeneous porous media with discontinuous capillary pressures*, Comput. Methods Appl. Mech. Eng. vol. 199 (23–24) (2010) pp. 1491–1501.
[20] H. Hoteit, A. Firoozabadi, *Numerical modeling of two-phase flow in heterogeneous permeable media with different capillarity pressures*, Adv. Water Resour. vol. 31(1) (2008) pp. 56–73.
[21] W. Klieber, B. Riviere, *Adaptive simulations of two-phase flow by discontinuous galerkin methods*, Comput. Methods Appl. Mech. Eng. vol. 196(1–3) (2006) pp. 404–419.
[22] J. Natvig, K. Lie, *Fast computation of multiphase flow in porous media by implicit discontinuous galerkin schemes with optimal ordering of elements*, J. Comput. Phys. vol. 227 (2008) pp. 10108–10124.
[23] A. Ern, I. Mozolevski, *Discontinuous galerkin method for two-component liquid–gas porous media flows*, Comput. Geosci. vol. 16(3) (2012) pp. 677–690.
[24] B. Riviere, X. Yang, *A new discontinuous galerkin method for the simulation of CO_2 injection in the saline aquifer*, Advances in the Mathematical Sciences, Springer, New York, USA, 2018.
[25] R. Rankin, B. Riviere, *A high order method for solving the black-oil problem in porous media*, Adv. Water Resour. vol. 78 (2015) pp. 126–144.
[26] I. Aavatsmark et al., *A compact multipoint flux approximation method with improved robustness*, Numer. Methods Partial Differ. Equ. vol. 24 (2008) pp. 1329–1360.
[27] A. S. Abushaikhaa, D. V. Voskov, H. A. Tchelepi, *Fully implicit mixed-hybrid finite-element discretization for general purpose subsurface reservoir simulation*, J. Comput. Phys. vol. 346 (2017) pp. 514–538.
[28] J. Moortgat, A. Firoozabadi, *Mixed-hybrid and vertex-discontinuous-Galerkin finite element modeling of multi-phase compositional flow on 3D unstructured grids*, J. Comput. Phys. vol. 315 (2016) pp. 476–500.
[29] G. Singh, M. Wheeler, *Compositional flow modeling using a multi-point flux mixed finite element method*, Comput. Geosci. vol. 20 (2016) pp. 421–435.
[30] H. Hajibeygi, H. A. Tchelepi, et al., *Compositional multiscale finite-volume formulation*, SPE J. vol. 19(02) (2014) pp. 316–326.
[31] P. Raviart, J. Thomas, "*Introduction to the numerical analysis of partial differential equations*," in *Collection Mathématiques Appliquées pour la Maîtrise*, Masson, Paris French, 1983.
[32] P. Bastian et al., *A generic grid interface for parallel and adaptive scientific computing. Part ii: Implementation and tests in dune*, Computing vol. 82(2–3) (2008) pp. 121–138.
[33] P. Bastian et al., *A generic grid interface for parallel and adaptive scientific computing. Part i: Abstract framework*, Computing vol. 82(2–3) (2008) pp. 103–119.
[34] M. Blatt, P. Bastian, *On the generic parallelisation of iterative solvers for the finite element method*, Int. J. Comput. Sci. Eng. vol. 4(1) (2008) pp. 56–69.
[35] M. Blatt et al., *The distributed and unified numerics environment, version 2.4*, Arch. Numer. Softw. vol. 4(100) (2016) pp. 13–29.
[36] R. G. Bentsen, J. Anli, *A new displacement capillary pressure model*, J. Can. Pet. Technol. vol. 15 (1976) pp. 75–79.
[37] Z. Chen, G. Huan, Y. Ma, *Computational methods for multiphase flows in porous media*, Society for Industrial and Applied Mathematics SIAM, Philadelphia, Pennsylvania, USA, 2006.
[38] R. Courant, K. Friedrichs, H. Lewy, *Über die partiellen differenzengleichungen der mathematischen physik*, Math. Ann. vol. 100(1) (1928) pp. 32–74.
[39] R. Brooks, T. Corey, *Hydraulic properties of porous media*, vol. 24, Hydrology Papers, Colorado State University, Fort Collins, Colorado, USA, 1964.
[40] K. Aziz, A. Settari, *Petroleum reservoir simulation*, Chapman & Hall, Boca Raton, Florida, USA, 1979.
[41] U. G. Araktingi, F. Orr Jr. et al., *Viscous fingering in heterogeneous porous media*, SPE Adv. Technol. Ser. vol. 1(01) (1993) pp. 71–80.
[42] J. Li, B. Rivière, *Numerical modeling of miscible viscous fingering instabilities by high-order methods*, Transp. Porous Media vol. 113(3) (2016) pp. 607–628.
[43] A. Riaz, E. Meiburg, *Vorticity interaction mechanisms in variable-viscosity heterogeneous miscible displacements with and without density contrast*, J. Fluid Mech. vol. 517 (2004) pp. 1–25.
[44] H. Tchelepi, F. Orr Jr.. , et al., *Interaction of viscous fingering, permeability heterogeneity, and gravity segregation in three dimensions*, SPE Reserv. Eng. vol. 9(04) (1994) pp. 266–271.
[45] P. Van Meurs, et al. *The use of transparent three-dimensional models for studying the mechanism of flow processes in oil reservoirs*. Society of Petroleum Engineers, Richardson, Texas, USA, 1957.

[46] P. Bastian, R. Helmig, *Efficient fully-coupled solution techniques for two-phase flow in porous media: Parallel multigrid solution and large scale computations*, Adv. Water Resour. vol. 23(3) (1999) pp. 199–216.
[47] W. Bangerth et al., *On optimization algorithms for the reservoir oil well placement problem*, Comput. Geosci. vol. 10(3) (2006) pp. 303–319.

How to cite this article: Cappanera L, Rivière B. Discontinuous Galerkin method for solving the black-oil problem in porous media. *Numer Methods Partial Differential Eq.* 2018;1–29. https://doi.org/10.1002/num.22324

APPENDIX A: NOMENCLATURE

TABLE A1 Nomenclature of physical variables. The phase i can either represent the liquid phase (i = l), the vapor phase (i = v) or the aqueous phase (i = a). The component j can either represent oil (j = o), gas (j = g) or water (j = w)

Notation	Physical quantity
ρ_i	Density of the phase i
p_i	Pressure of the phase i
$p_{c,v}$	Vapor capillary pressure
$p_{c,a}$	Aqueous capillary pressure
$x_{j,i}$	Mass fraction of component j in phase i
λ_i	Mobility of the phase i
μ_i	Viscosity of the phase i
κ_i	Relative permeability of the phase i
κ_{abs}	Absolute permeability
S_i	Saturation of phase i
z_g	Total fraction of gas
q_i	Source term related to the phase i
ϕ	Porosity
$\mathbf{g}$	Gravity

APPENDIX B: DETAILS ON THE COMPUTATION OF SOME PARTIAL DERIVATIVES

This appendix aims to provide information necessary for the correct implementation of the algorithm described in Section 3. It focuses on describing how the variables $\frac{\partial F_g}{\partial z_g}$ and the partial derivatives of the liquid and vapor saturations are computed.

B.1 | Computation of $\frac{\partial F_g}{\partial z_g}$

To compute the derivative $\frac{\partial F_g}{\partial z_g}$, we rewrite F_g as a function of z_g. We assume that the relative permeability κ_ℓ, respectively κ_v and κ_a, is a differentiable function of S_ℓ and S_a, respectively of S_v and S_a.

We can write:

$$\kappa_l = \kappa_\ell(S_\ell, S_a), \qquad \kappa_v = \kappa_v(S_v) \qquad \text{and} \qquad \kappa_a = \kappa_a(S_a). \tag{B.1}$$

The definition of F_g can be rewritten as follows:

$$F_g = \mu_a \frac{x_{g,\ell}\mu_v\rho_\ell\kappa_\ell(S_\ell, S_a) + x_{g,v}\mu_\ell\rho_v\kappa_v(S_v)}{\mu_a\mu_v\rho_\ell\kappa_\ell(S_\ell, S_a) + \mu_a\mu_\ell\rho_v\kappa_v(S_v) + \mu_\ell\mu_v\rho_a\kappa_a(S_a)}.$$

As S_ℓ and S_v are functions of the variable z_g, see Equations (3.13) and (3.14), we can compute the derivative $\frac{\partial F_g}{\partial z_g}$ as follows:

$$\begin{aligned}\frac{\partial F_g}{\partial z_g} = x_{g,\ell} &\frac{\mu_a^2\mu_\ell\mu_v\rho_\ell\rho_v\left(\kappa_v(S_v)\frac{\partial\kappa_\ell}{\partial S_\ell}(S_\ell, S_a)\frac{\partial S_\ell}{\partial z_g} - \kappa_\ell(S_\ell, S_a)\kappa_v'(S_v)\frac{\partial S_v}{\partial z_g}\right) + \mu_a\mu_\ell\mu_v^2\rho_a\rho_\ell\kappa_a(S_a)\frac{\partial\kappa_\ell}{\partial S_\ell}(S_\ell, S_a)\frac{\partial S_\ell}{\partial z_g}}{(\mu_a\mu_v\rho_\ell\kappa_\ell(S_\ell, S_a) + \mu_a\mu_\ell\rho_v\kappa_v(S_v) + \mu_\ell\mu_v\rho_a\kappa_a(S_a))^2} \\ + x_{g,v} &\frac{\mu_a^2\mu_\ell\mu_v\rho_\ell\rho_v\left(\kappa_\ell(S_\ell S_a)\kappa_v'(S_v)\frac{\partial S_v}{\partial z_g} - \kappa_v(S_v)\frac{\partial\kappa_\ell}{\partial S_\ell}(S_\ell, S_a)\frac{\partial S_\ell}{\partial z_g}\right) + \mu_a\mu_\ell^2\mu_v\rho_a\rho_v\kappa_a(S_a)\kappa_v'(S_v)\frac{\partial S_v}{\partial z_g}}{(\mu_a\mu_v\rho_\ell\kappa_\ell(S_\ell, S_a) + \mu_a\mu_\ell\rho_v\kappa_v(S_v) + \mu_\ell\mu_v\rho_a\kappa_a(S_a))^2}.\end{aligned}$$

We note that the term $\frac{\partial S_v}{\partial z_g}$ can be replaced by $-\frac{\partial S_\ell}{\partial z_g}$ in the above formula. It reads:

$$\begin{aligned}\frac{\partial F_g}{\partial z_g} = &\frac{\mu_a^2\mu_\ell\mu_v\rho_\ell\rho_v(x_{g,\ell} - x_{g,v})\left(\kappa_v(S_v)\frac{\partial\kappa_\ell}{\partial S_\ell}(S_\ell, S_a) + \kappa_\ell(S_\ell)\kappa_v'(S_v)\right)\frac{\partial S_\ell}{\partial z_g}}{(\mu_a\mu_v\rho_\ell\kappa_\ell(S_\ell, S_a) + \mu_a\mu_\ell\rho_v\kappa_v(S_v) + \mu_\ell\mu_v\rho_a\kappa_a(S_a))^2} \\ &+ \frac{\mu_a\mu_\ell\mu_v\rho_a\left(x_{g,\ell}\mu_v\rho_\ell\frac{\partial\kappa_\ell}{\partial S_\ell}(S_\ell, S_a) - x_{g,v}\mu_\ell\rho_v\kappa_v'(S_v)\right)\frac{\partial S_\ell}{\partial z_g}\kappa_a(S_a)}{(\mu_a\mu_v\rho_\ell\kappa_\ell(S_\ell, S_a) + \mu_a\mu_\ell\rho_v\kappa_v(S_v) + \mu_\ell\mu_v\rho_a\kappa_a(S_a))^2}.\end{aligned} \tag{B.2}$$

B.2 | Derivatives of the saturations S_ℓ and S_v with respect to z_g

The quantities $\frac{\partial S_\ell}{\partial z_g}$ and $\frac{\partial S_v}{\partial z_g}$ can be derived from Equations (3.13) and (3.14):

$$\frac{\partial S_\ell}{\partial z_g} = \frac{-\rho_\ell\rho_v(x_{g,v} - x_{g,\ell})(1 - S_a) - \rho_a(\rho_v x_{g,v} - \rho_\ell x_{g,\ell})S_a}{((x_{g,v} - z_g)\rho_v + (z_g - x_{g,\ell})\rho_\ell)^2}, \tag{B.3}$$

$$\frac{\partial S_v}{\partial z_g} = \frac{\rho_\ell\rho_v(x_{g,v} - x_{g,\ell})(1 - S_a) + \rho_a(\rho_v x_{g,v} - \rho_\ell x_{g,\ell})S_a}{((x_{g,v} - z_g)\rho_v + (z_g - x_{g,\ell})\rho_\ell)^2}. \tag{B.4}$$

The terms $\frac{\partial S_v}{\partial z_g}^+$ and $\frac{\partial S_v}{\partial z_g}^-$ used in Equation (3.10) are defined as follows:

$$\left(\frac{\partial S_v}{\partial z_g}\right)^+ = \frac{\rho_\ell\rho_v(x_{g,v} - x_{g,\ell})(1 - S_a) + \rho_a\rho_v x_{g,v}S_a}{((x_{g,v} - z_g)\rho_v + (z_g - x_{g,\ell})\rho_\ell)^2}, \tag{B.5}$$

$$\left(\frac{\partial S_v}{\partial z_g}\right)^- = \frac{-\rho_a\rho_\ell x_{g,\ell}S_a}{((x_{g,v} - z_g)\rho_v + (z_g - x_{g,\ell})\rho_\ell)^2}. \tag{B.6}$$

B.3 | Other partial derivatives involving the saturation S_v

The terms $\frac{\partial S_v}{\partial x_{g,\ell}}$, $\frac{\partial S_v}{\partial x_{g,\ell}}$, $\frac{\partial S_v}{\partial \rho_\ell}$, $\frac{\partial S_v}{\partial \rho_v}$ and $\frac{\partial S_v}{\partial \rho_a}$ used in Equation (3.10) can be derived from Equation (3.14). We have:

$$\frac{\partial S_v}{\partial x_{g,\ell}} = \frac{\rho_\ell(\rho_v(1 - S_a)(z_g - x_{g,v}) + \rho_a S_a z_g)}{((x_{g,v} - z_g)\rho_v + (z_g - x_{g,\ell})\rho_\ell)^2}, \tag{B.7}$$

$$\frac{\partial S_v}{\partial x_{g,v}} = \frac{-\rho_v(\rho_\ell(-1+S_a)(x_{g,\ell}-z_g)+\rho_a S_a z_g)}{((x_{g,v}-z_g)\rho_v+(z_g-x_{g,\ell})\rho_\ell)^2}, \tag{B.8}$$

$$\frac{\partial S_v}{\partial \rho_\ell} = \frac{-(x_{g,\ell}-z_g)(\rho_v(1-S_a)(x_{g,v}-z_g)-\rho_a S_a z_g)}{((x_{g,v}-z_g)\rho_v+(z_g-x_{g,\ell})\rho_\ell)^2}, \tag{B.9}$$

$$\frac{\partial S_v}{\partial \rho_v} = \frac{-(x_{g,v}-z_g)(\rho_\ell(1-S_a)(z_g-x_{g,\ell})+\rho_a S_a z_g)}{((x_{g,v}-z_g)\rho_v+(z_g-x_{g,\ell})\rho_\ell)^2}, \tag{B.10}$$

$$\frac{\partial S_v}{\partial \rho_a} = \frac{S_a z_g}{(x_{g,v}-z_g)\rho_v+(z_g-x_{g,\ell})\rho_\ell}. \tag{B.11}$$